Status of the K500 and K800 Cyclotrons
Project Staff (Report by D. Clark)

This section summarizes the status of the K500 and K800 cyclotron construction as of November 1980. A number of photographs are included to illustrate the project activities. Some detailed articles follow describing various parts of the R&D and construction programs.

The K500 Cyclotron

The K500 Cyclotron major sub-systems are in the final fabrication and installation phases. The magnet is assembled and ready for final magnetic field measurements. The magnet coil and refrigeration systems have been operated successfully over the past 3 years, with 10 liquid helium cool-downs, and constitute a reliably operating subsystem of the cyclotron. One rf prototype amplifier, resonator and dee system has operated at design dee voltage, and the final systems are under construction. Extensive prototype testing has been successfully completed on other sub-systems including the ion source (reported previously), and the cryopumping and deflector high voltage systems (described in later articles in this section).

The magnet operating range was increased from the original design value of 700 amps/turn (3500 amps/cm^2 average current density) to 800 amps/turn (4000 amps/cm^2). This gives a wider range of magnet field trimming with the two independent sections of the main coil, and reduces total trim coil power. In early 1980 the main magnet was disassembled for installation of the median plane penetrations through the coil system. These penetrations contain supports for the extraction element and compensating bar radial positioning, the voltage feeds for the two sections of electrostatic deflector, probe port, and extracted beam channel. Modifications were made in the pole tip iron. Holes were drilled in the poles adjacent to the hills to bring the 13 pairs of leads out the top and bottom of the magnet from the 13 trimming coils on each hill surface. Holes were also drilled through the poles for rf trimming and coupling capacitors at the dees. Final iron shimming to obtain the optimum radial profile was done on the pole faces. The 13 sets of trimming coils on each hill were potted on the upper hills (close to the midplane) and water flow tested. They were then installed on the poles.

The coil cryostat system was reassembled by wrapping the coil bobbin with superinsulation, installing the aluminum liquid nitrogen shield, wrapping again with superinsulation, and installing this assembly inside the room temperature outer housing. The penetration tubes were then installed through the midplane, insulated with superinsulation, and welded in place. The coil cryostat welds were carefully leak checked. Then the coil system was installed in the lower magnet yoke and the magnet was reassembled. The cryostat was filled with liquid helium, and the boiloff rate was found to be comparable to previous runs without the midplane penetrations. The refrigerator handled the load well. The leak rate into the cryostat vacuum was so low that for the first time this vacuum could be isolated and pumped by the cryostat itself. So the insulation and leak hunting were very successful.

The analysis of the last set of field measurements[1] laid the foundation for the final magnetic shimming calculations.[2] Extensive orbit calculations were then done in the region before extraction[3] and in the extraction channel.[4] The final pole tip shimming was calculated to compensate the holes in the poles for trim coil leads and rf feedthroughs. Also an improved shimming was designed for the average field of the centerplug, and to increase the focusing slightly at large radius. Orbit tracking of phase space ellipses was done for 8 representative beams throughout the operating range to determine optimum first harmonic bumps for extraction. Adequate turn separation of at least 1 mm between ellipses was obtained, with good beam quality. The $\nu_r+2\nu_z=3$ resonance was observed to cause vertical beam blowup prior to extraction when a first harmonic bump was used and the average field was low (about 30 kG). The appearance of this resonance at low field is due to the constant field modulation of the saturated sectors causing an increase in ν_z. As a result, it appears that the minimum operating field will be about 30 kG. This does not restrict the energy range for heavy ions, since ion charge can be selected for different energy regions. The calculations also showed that the extraction radius, and thus the radial position of the extraction elements should be varied with the operating point. Detailed extraction calculations were also done, and show good beam quality using 2 electrostatic channels and 9 sets of magnetic focusing bars. Electrostatic fields in the deflectors are conservative (<135 kV/cm with a gap of 7-8 mm). The first harmonic due to the magnetic channels

is compensated by movable compensating iron bars. Various beams have different envelopes through the extraction system, but all pass through a common point in an external steering magnet, where they are centered on the following beam line. Then a system of quadrupoles matches the various beam emittance shapes to a common emittance shape at a downstream slit.

The final field measurements will commence in late 1980 and are expected to take about 2 months. They will begin just after the centering of the coil to equalize the link forces, and the centering of the cryostat to minimize the magnetic first harmonic. The final complete set of median plane field measurements will be taken at many field levels. This set of measurements will be on the final magnetic field, because the magnetic focusing bars and final pole face shimming will be in place, and the effect of each of the recently installed trim coils will be measured. The arm with 55 flip coils will be used again, with better calibration of the coils.

The development of the rf system for the K500 is proceeding well. Extensive tests have been run of the performance of one transmitter into a simulated dee in vacuum, and attached dee stems. 100 kV has been obtained on the dee for 24 hours, and frequencies spanning the operating range have been run. The moving short has evolved into a reliable design using air cylinders on contact springs on the inner conductor and air bellows on contact fingers on the outer conductor. Construction is proceeding on the other two transmitters, and the stems for tuning the dees and transmitters.

Studies are continuing on the center region first and second harmonic modes of acceleration. Recent improvements have been made on the speed and accuracy of the electrolytic tank. The accuracy was checked on a case of eccentric cylinders, where an analytical solution existed.

The K800 Cyclotron

The K800 Cyclotron to be constructed as part of Phase II is in the early design stage. Sufficient magnetic field and orbit calculations have been done[5,6] to finalize the specifications for the magnet, pole tips, main coils and trim coils. The large components have been ordered. The main coil conductor and bobbin are due in March 1981, and the 10 foot lathe for winding the coil has been received. The delivery of the magnet steel is expected in late 1981. The main 1.2 megawatt d.c. power supply for the rf system and the helium refrigerator/liquifier will arrive in 1981. The 3600 gallon surplus LN_2 tanks have been renovated and erected to supply the project requirements. The building addition to house the K800 vault, and expanded experimental area and office space is under construction, and will be completed in early 1982.

A recent modification in the magnet design is an increase in the coil distance from the median plane from 1.5 inches to 2.0 inches to provide more axial space for extraction elements. Preliminary force calculations show that in the extreme cases the force on the coil nearest the median plane is up to 2100 tons toward the midplane, while the force on the coil away from the median plane ranges from 900 tons away from the midplane when the polarity is negative (bucking the other coil), to 2300 tons toward the midplane for positive polarity. The hoop stress in the superconducting cable for an extreme case is 8000 psi, i.e. considerably less than the safe limit at 15,000 psi. The rf system for the K800 has been designed. A half scale model of the dee will be built to calculate the performance and power requirements of the resonators. A final transmitter tube has been purchased to make preliminary tests.

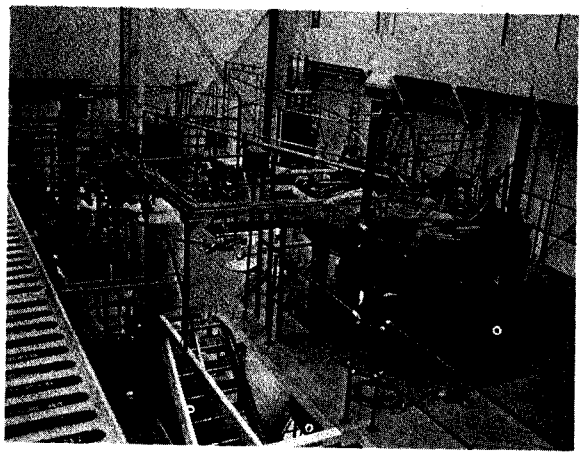

FIG. 1. View of the magnet of the K500 from the upper level with top raised for access. Magnet was later dis-assembled for installation of median plane penetrations. Shielding walls are being installed at the locations defined by the edges of the metal deck.

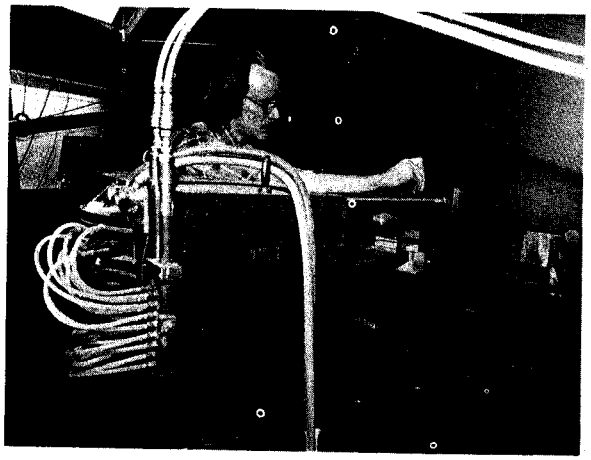

FIG. 2. Mapping of the fringing field of the K500 magnet in the vicinity of the extraction channel. The final set of "focusing bars" is located in the hole in the magnet yoke just below the worker's hand. The steering magnet at left center is the first element of the beam transport system.

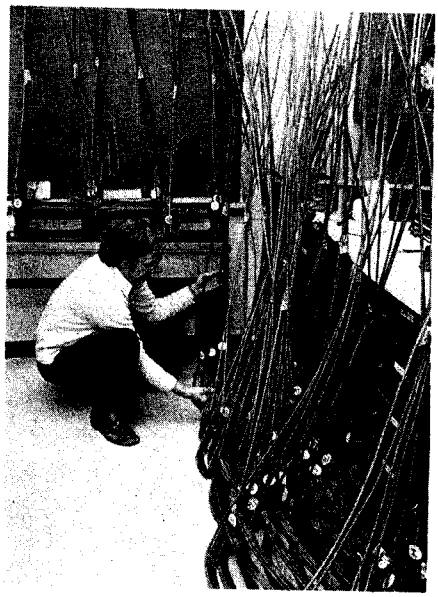

FIG. 3. Room temperature trimming windings for the cyclotron waiting to be installed on the pole tips.

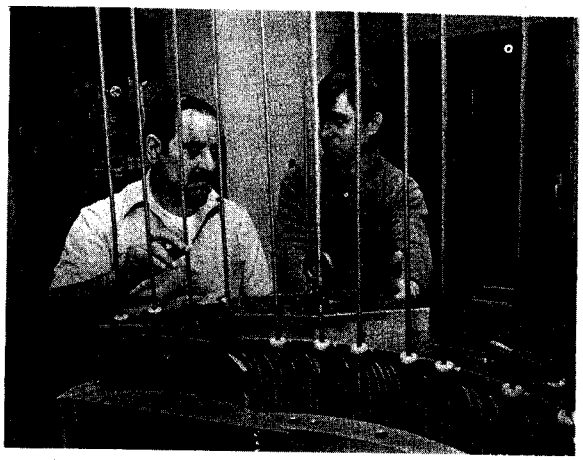

FIG. 4. An outer pole tip section with its seven trimming windings as it is being lowered into the vacuum potting fixture.

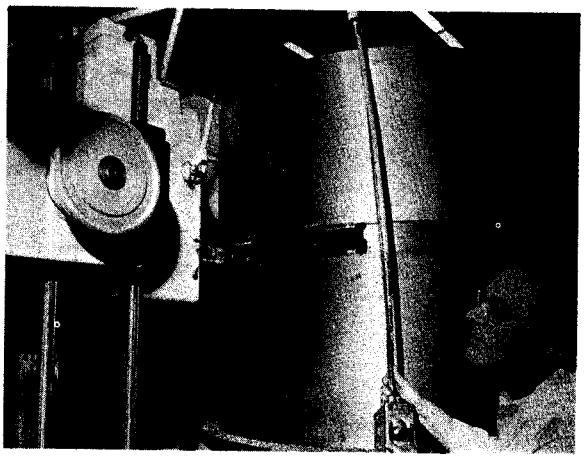

FIG. 5. Milling the extraction channel opening in the inner cryostat wall.

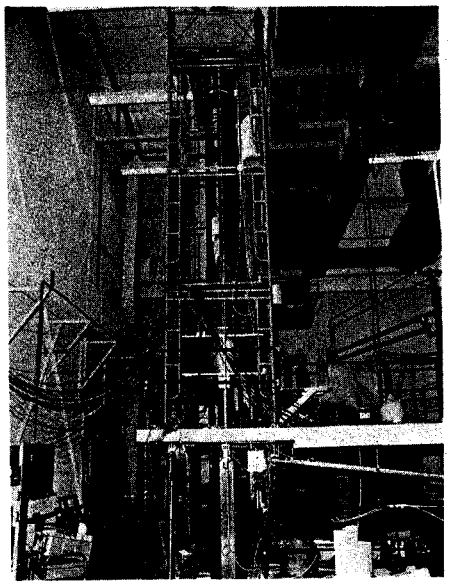

FIG. 6. Photograph of the prototype resonator set up for high power RF tests. The prototype dee is housed in a dummy aluminum vacuum chamber, the exterior of which is visible just below the center of the picture.

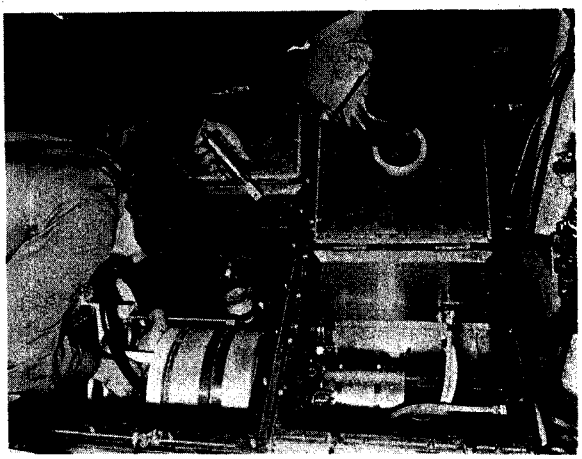

FIG. 8. Power amplifier No. 1 with access doors open to the grid box at the top and the plate box at the bottom.

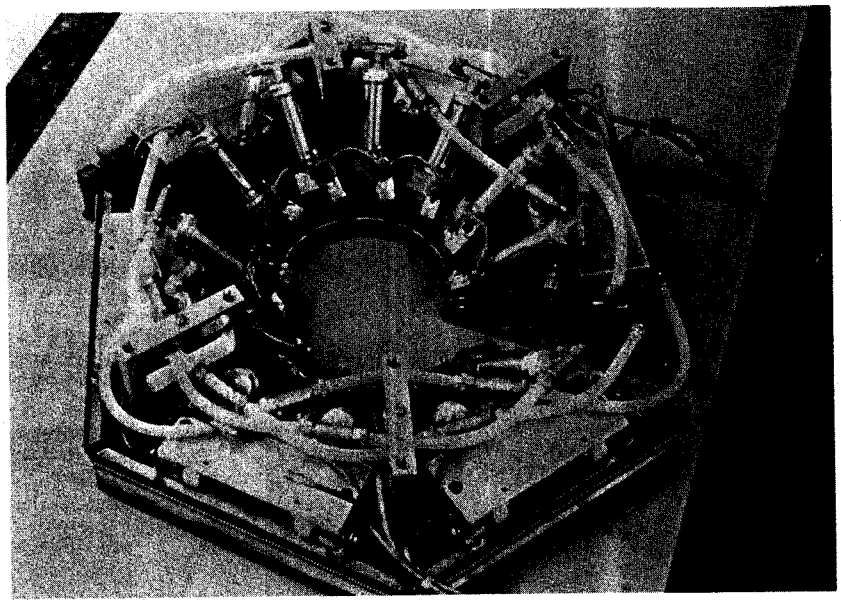

FIG. 7. Sliding short for dee stem, showing 12 air cylinders which clamp RF contact springs against inner cylindrical conductor of dee stem when short reaches desired position. Outer 6 sets of contact fingers are clamped against hexagonal outer dee stem conductor by bellows cylinders under outer plates.

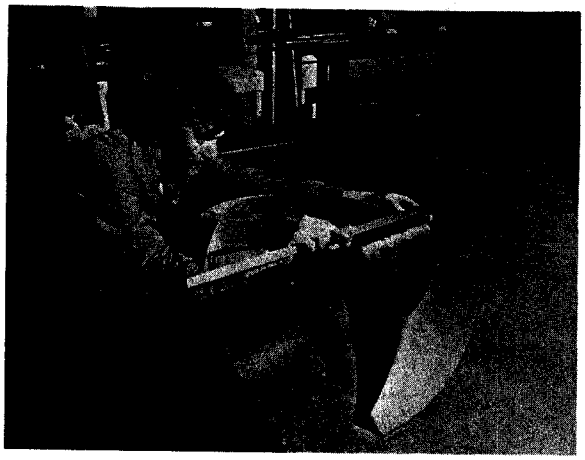

FIG. 9. Upper half of a dee in preparation for locating the dee stem attachment collar.

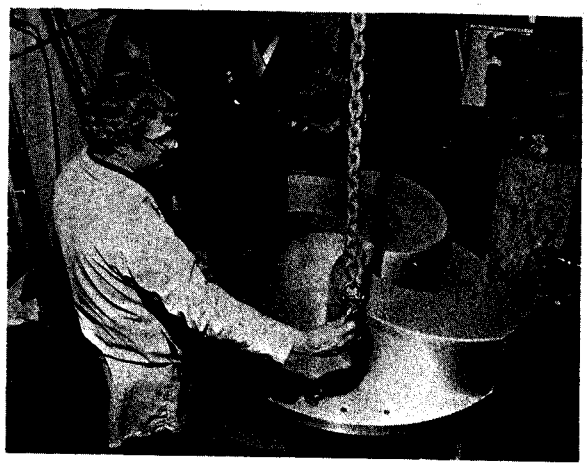

FIG. 11. The set of aluminum pole tips which will be used as a "hammer form" in fabricating the copper liner structure. This liner will completely cover the poles and isolate the trimming coils in a separate vacuum envelope.

FIG. 10. Prototype cryopumping panel being set up for tests in a rectangular dummy aluminum vacuum box. The panel will ultimately mount inside the dee. The outer crescent shaped box in the figure will be at 80 ° K and contains the 4.5 ° K pumping panel. The chevron in the workers's hand faces the beam space and shields the 4.5 ° K surface.

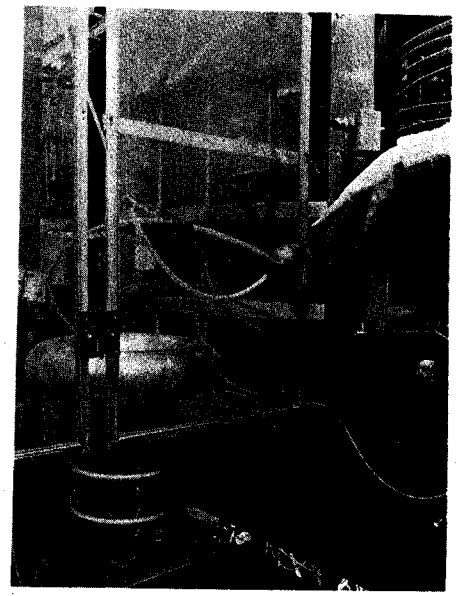

FIG. 12. A 150 kV deflector power supply for the K500 under test on the deflector of the 50 MeV cyclotron.

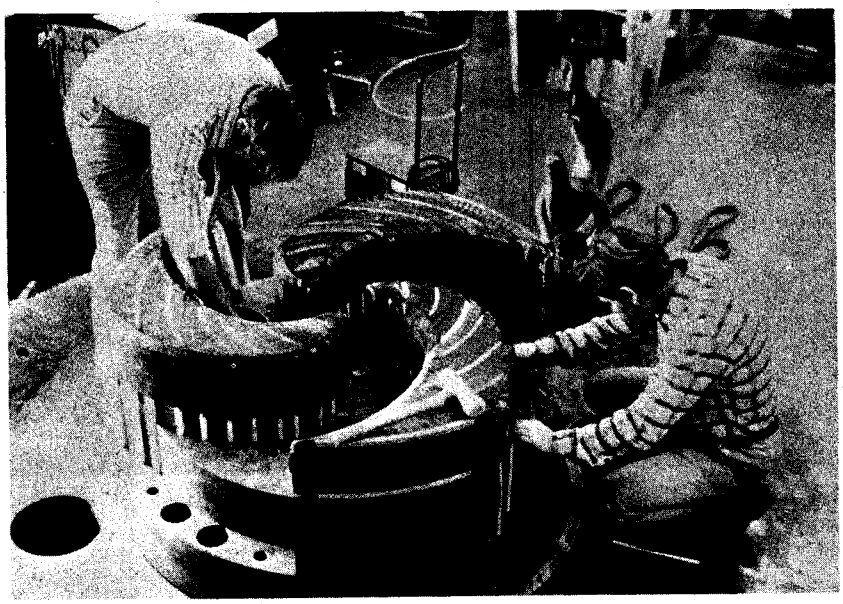

FIG. 13. Installation of spiral iron pole tips with their trim coils on lower pole cap. Trim coil leads pass through holes in pole.

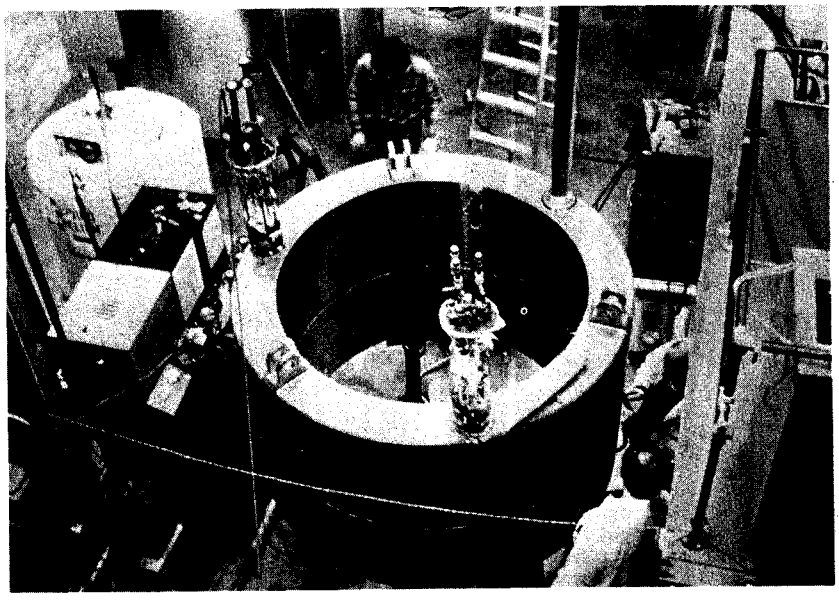

FIG. 14. Superconducting coil bobbin of stainless steel which has been welded shut to contain liquid helium. On top of bobbin are seen the 3 clevises for the support links, and other ports for helium feed, current leads, and venting. 20 layers of superinsulation will be wrapped around bobbin.

FIG. 15. Aluminum heat shield to be installed between 4° K superconducting coil and outer room temperature wall. It will run at liquid nitrogen temperature.

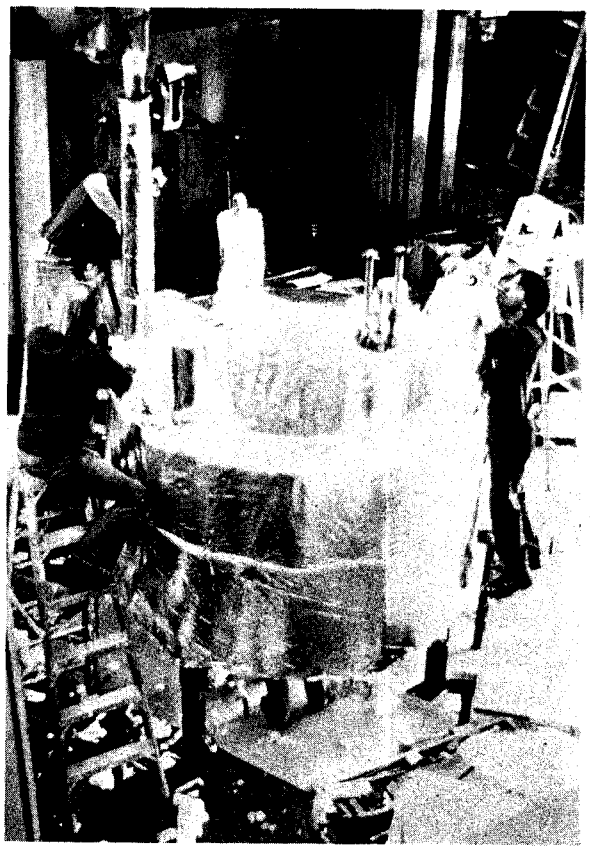

FIG. 16. Heat shield installed around bobbin. 20 layers of superinsulation insulate the shield.

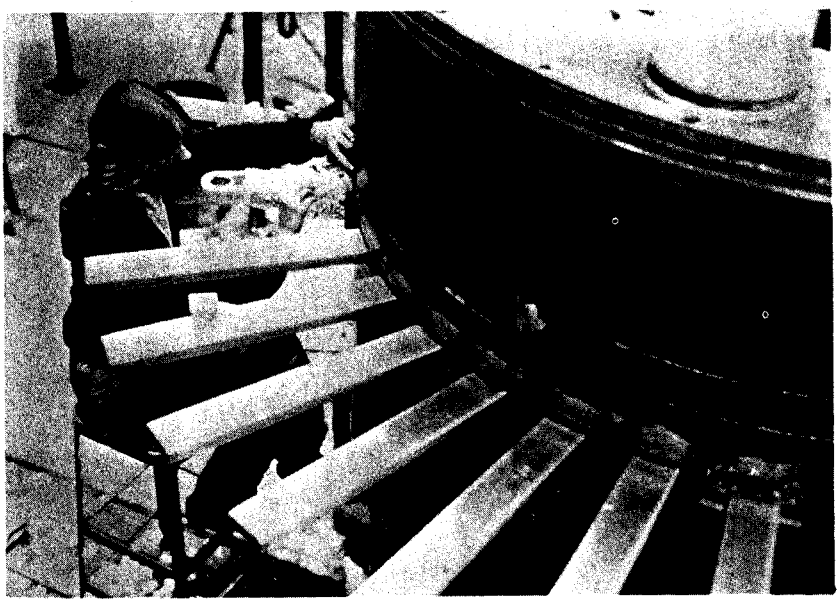

FIG. 17. Median plane extraction tubes shown penetrating the outer room temperature wall of the coil cryostat. Insulation is being done on one of the radial support links of the coil.

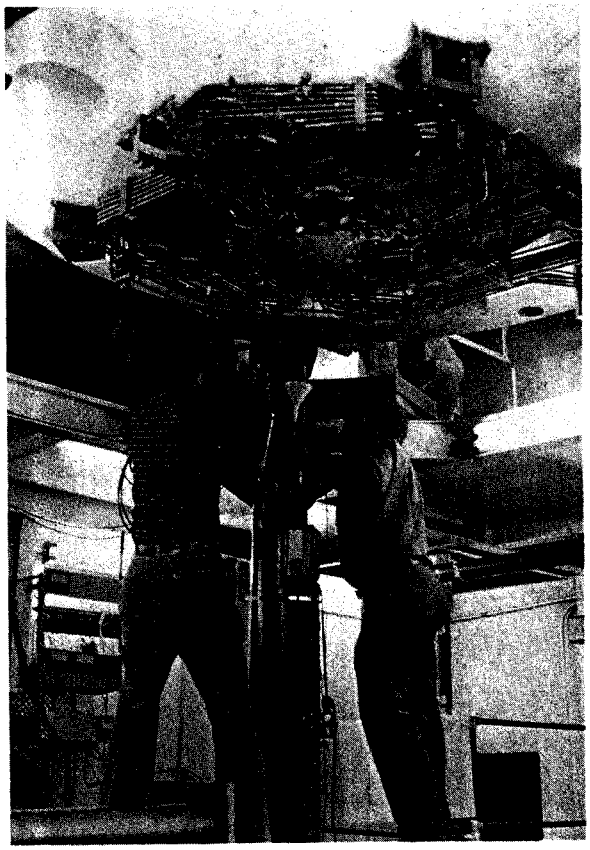

FIG. 18. Bottom cap of K500 cyclotron magnet being installed on support posts in the pit after completion of copper piping on cap to feed current and water to lower trimming coils.

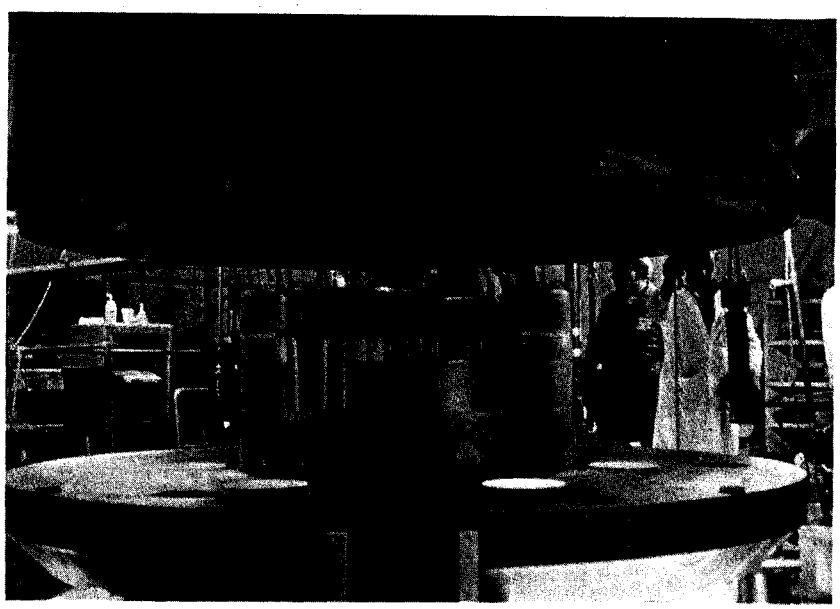

FIG. 19. Lower iron return path ring being lowered onto lower pole cap. Lower iron hills with trim coils are seen at center.

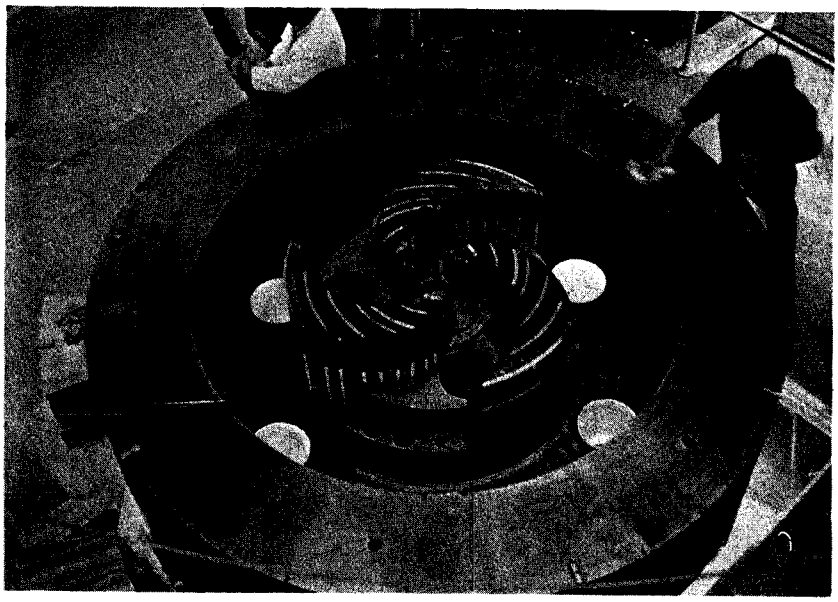

FIG. 20. Lower iron return path ring in place around lower pole. Lower spiral iron hills with their trimming coils on top are seen at center. Dee stem holes are visible between hills.

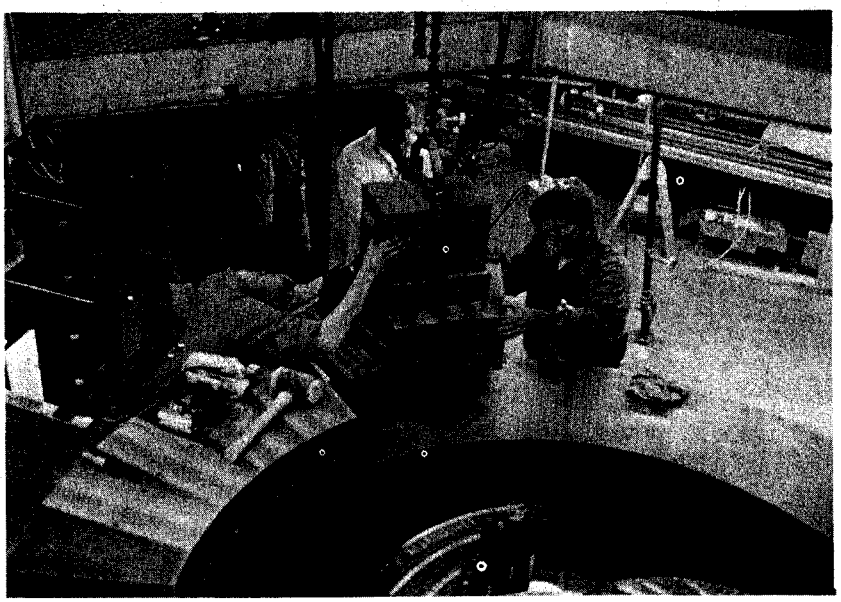

FIG. 21. Installation of iron median plane return path sections with magnetic lifting fixture. Rectangular holes in sections are for extraction elements.

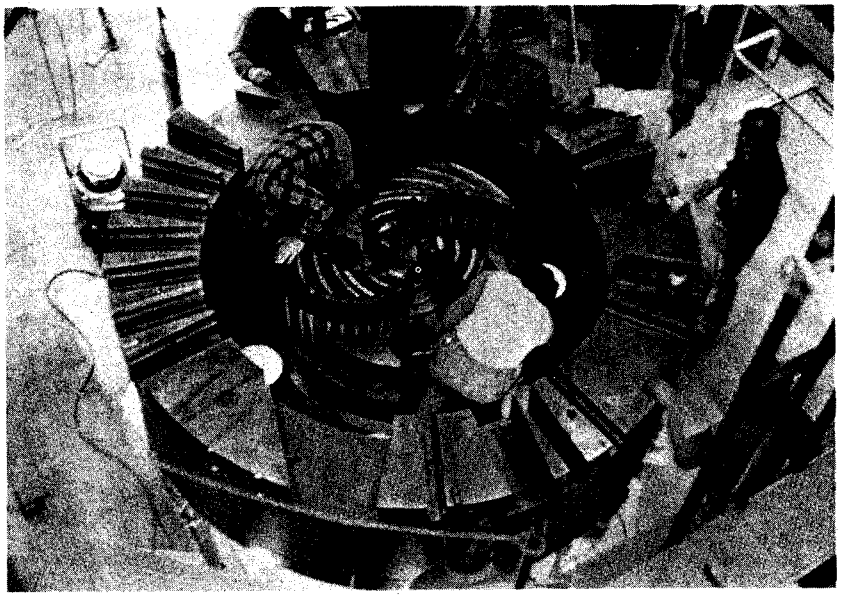

FIG. 22. Lower half of magnet with iron median plane sections in place. Vacuum gasket ring in lower cap is being installed.

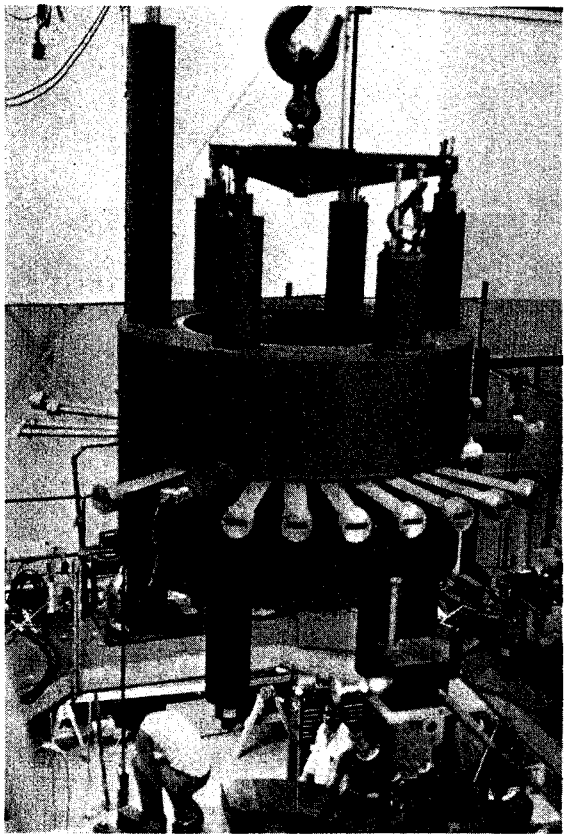

FIG. 23. Coil assembly on crane hook, ready for lowering into lower half of magnet yoke. Median plane tubes at center and right are for magnetic extraction bars.

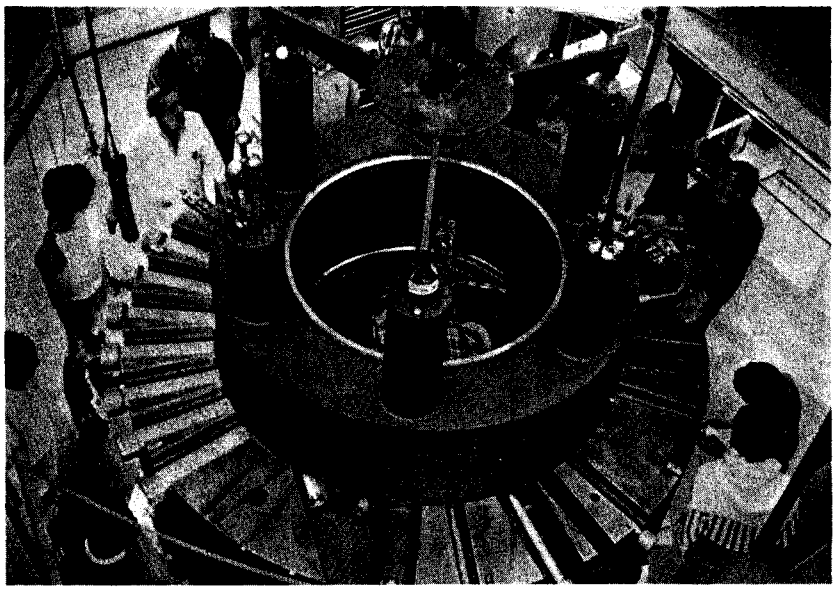

FIG. 24. Coil assembly in final position on lower half of magnet. Electrostatic extraction penetrations are at lower right, magnetic channel pipes are at left, and extracted beam tube is at bottom.

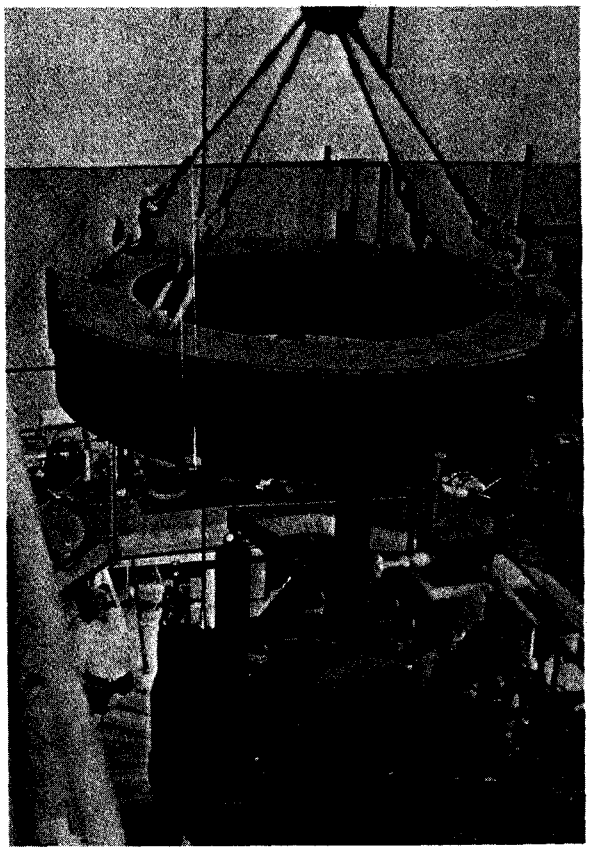

FIG. 25. Lowering upper iron return path ring over coil assembly.

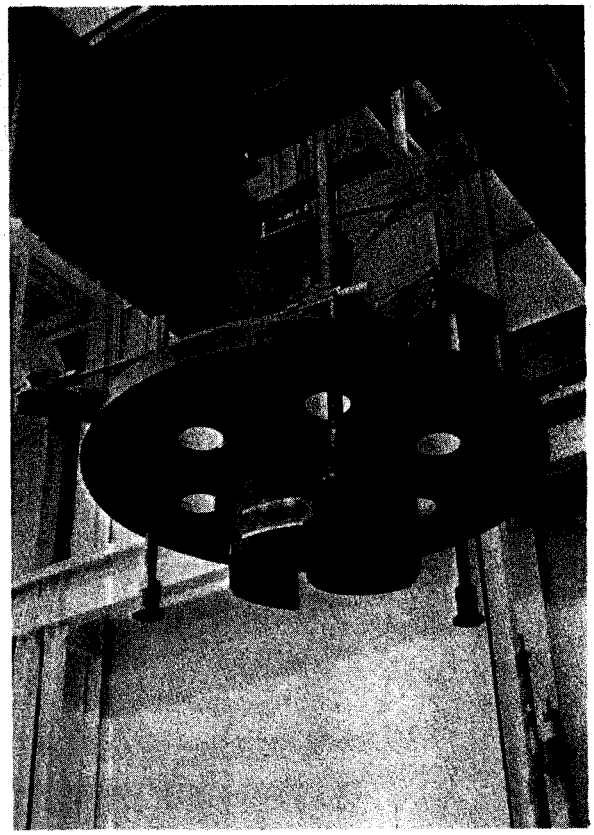

FIG. 26. Upper pole cap with its spiral iron sectors and trim coils being lowered with crane onto magnet.

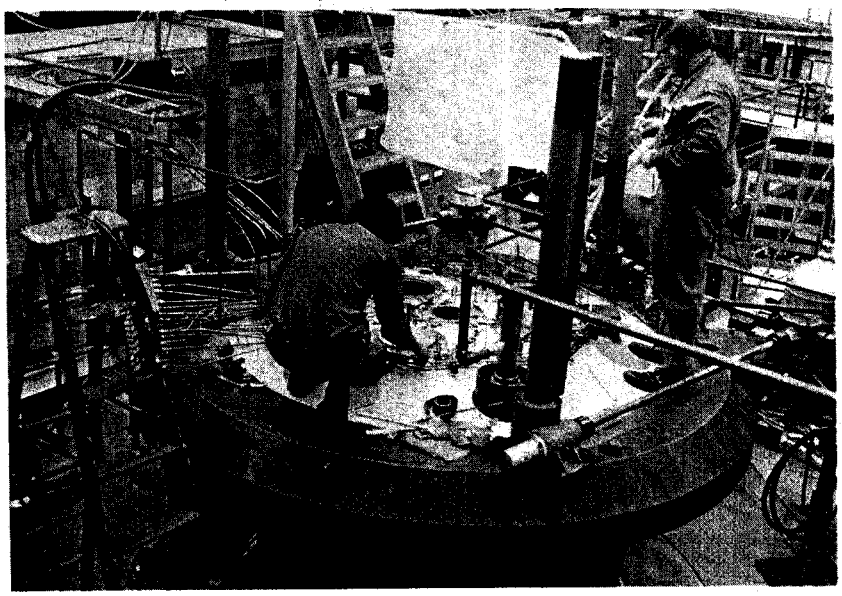

FIG. 27. Installation of trimming coil leads on top pole cap. Pole is in raised position.

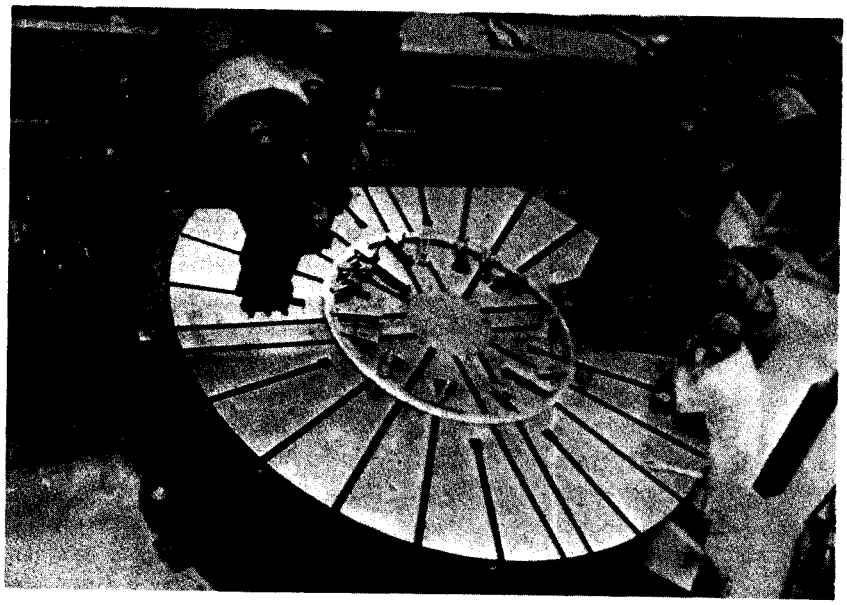

FIG. 28. Recently acquired 10 foot vertical lathe, to be used for winding the K800 cyclotron coil. It is being used here to machine a gasket ring for the K500 cyclotron.

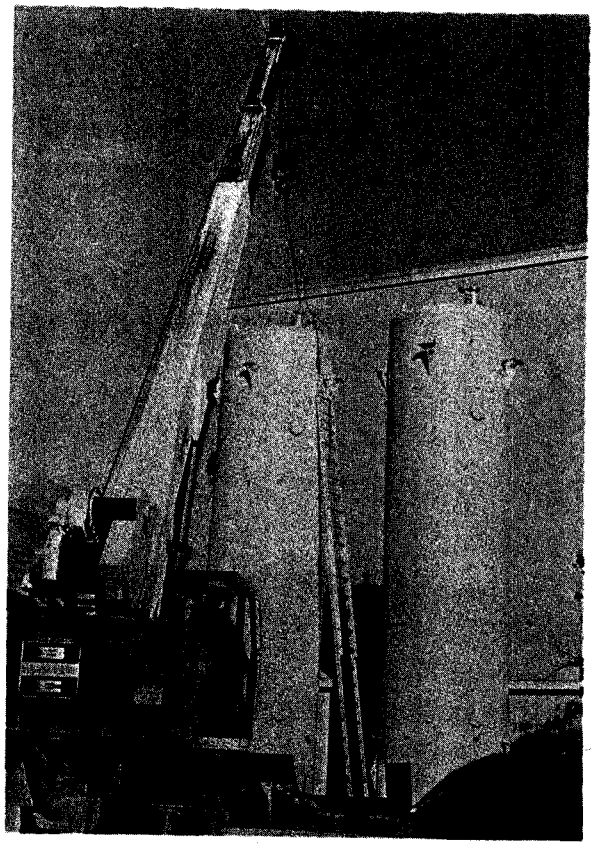

FIG. 29. Completion of erection of liquid nitrogen tanks for supplying building. They hold 3600 gallons each, and are 30 feet tall. They were obtained on surplus and were originally liquid oxygen missile silo tanks.

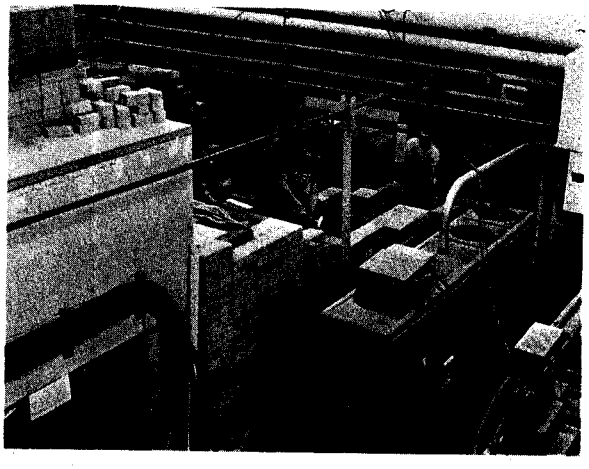

FIG. 30. Student workers in the process of reconfiguring the shielding wall for the Phase I beam transport system.

1. G. Bellomo, E. Fabrici, D. Johnson and F. Resmini, MSUCP-30, June 1980.
2. G. Bellomo, D. Johnson, P. Miller and F. Resmini, MSUCP-31, June 1980.
3. E. Fabrici and F. Resmini, MSUCP-32, June 1980.
4. E. Fabrici, D. Johnson and F. Resmini, MSUCP-33, June 1980.
5. Conceptual Design Report for Phase II of a National Superconducting Cyclotron Laboratory for Research with Heavy Ions, MSUCL-282, December 1978.
6. G. Bellomo, E. Fabrici, D. Johnson and F. Resmini, MSUCP-29, June 1980.

Building Addition to National Superconducting Cyclotron Laboratory

G.M. Crawley and J. Easley

One of the first steps in preparing for Phase II operation will be the construction of an addition to the present Laboratory building. (Figure 1) The total area of the new building will be approximately 38,000 square feet, and in addition about 3,500 square feet of the existing building will be modified. Additions will be made to the high bay both to the east and to the west and a major addition will be made to the office, data handling and computor areas. (See Figure 2).

The western addition to the high bay (about 60' x 77') will primarily house the K800 cyclotron and its associated equipment. The machine will be located over the pit in the southwest corner of the building. Poured concrete walls on the south and west sides near the machine will provide permanent shielding. An elevator to provide access to all 3 floors of the existing building will also be located in the north wall. This addition will also completely close off the central courtyard which will then be roofed over and winterised to provide more meeting and discussion space. The eastern addition to the high bay area (approximately 100' x 77') will provide new experimental areas including a pit to house a large magnetic spectrometer. A number of poured concrete walls (shown in heavy black in Fig. 2) will provide permanent shielding in these areas.

The office addition of approximately 16,600 square feet will include a seminar room, eleven new offices, plus a large open office area. This open plan office has been successfully

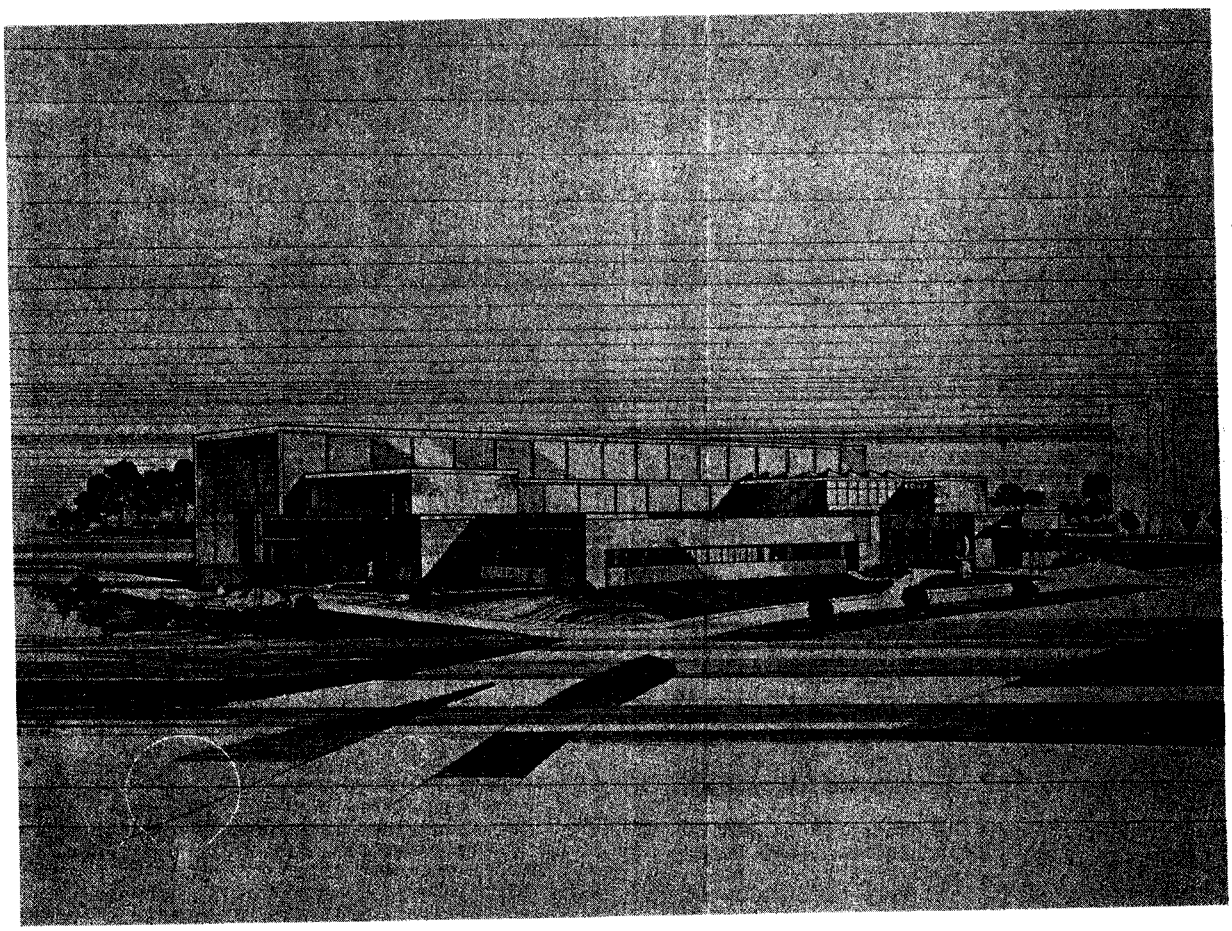

FIG. 1. Perspective of the new NSCL building from the Northeast.

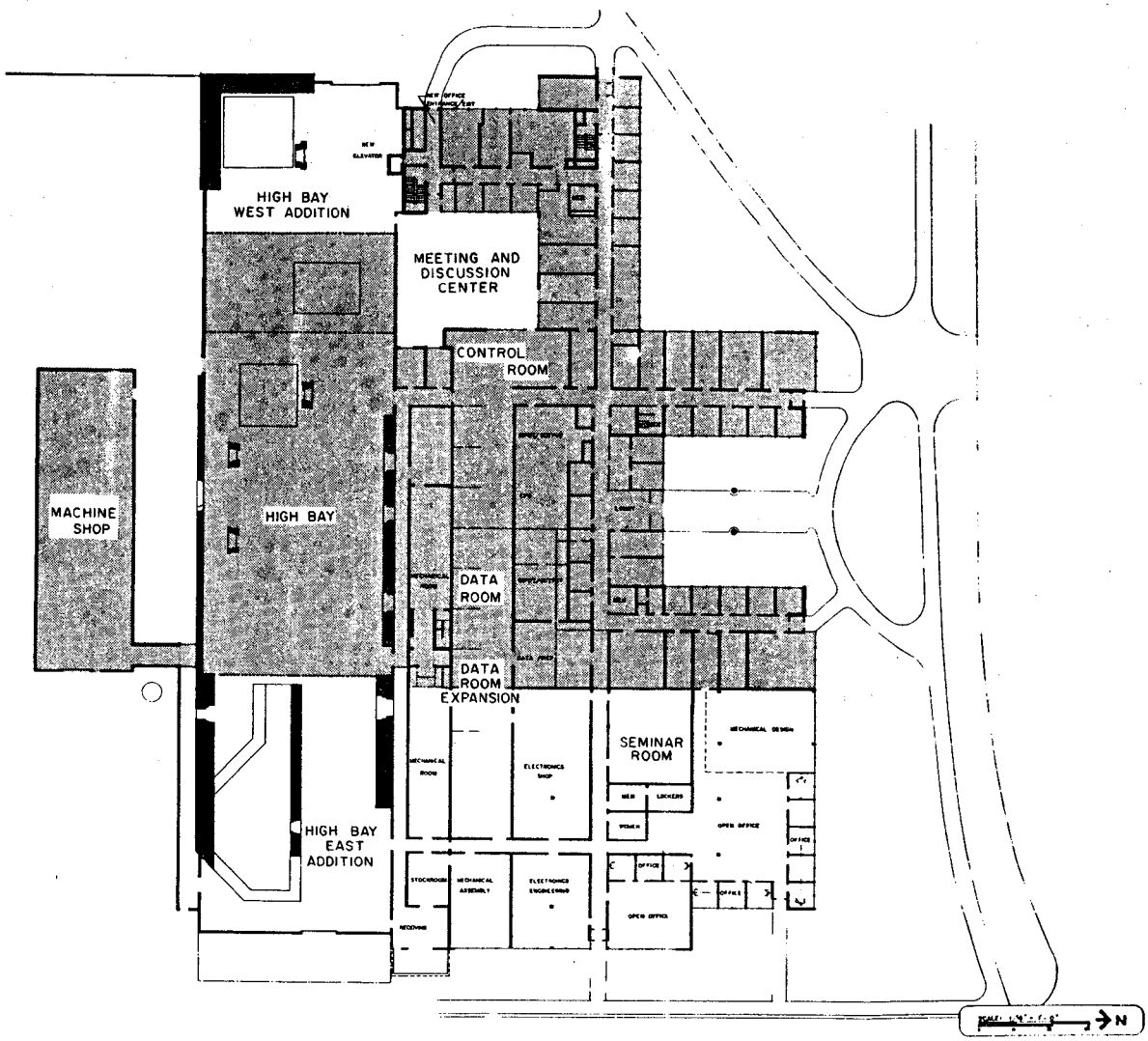

FIG. 2. Floor plan of the new building. The original building is shown shaded. Black regions are poured concrete walls for shielding.

implemented in the office area in the northeast corner of the existing building and makes very efficient use of space. The data room and computor space particularly for data preparation and handling will also be substantially expanded with the new addition. Much of the mechanical assembly, electronics shop and electronics engineering will probably also occupy space in the new building.

The contract for the construction of the building addition was signed with Foster, Schermerhorn, Barnes, Inc. in November 1980. Gilbert Commonwealth Companies are the architects for the building addition. The contract calls for occupancy of the west addition to the high bay by July 1, 1981 and occupancy of the remainder of the building by April 1, 1982. Work began on Nov. 17, 1980.

K500 Cryopanels

M. Mallory, H. Laumer, D. Poe, P. Brindza, D. Lawton and J. Ottarson

A prototype cryopanel for the K500 has been constructed and tested during the past year. The cryopanels will be mounted inside the dee and this necessitates the construction of coaxial transfer lines (17 ft) through the rf center conductor stems. Figure 1 is a drawing of the cryopanel and a cross section of the transfer lines. A vacuum space is inserted between the feed and return line of both the liquid helium and liquid nitrogen system in the transfer lines thereby avoiding heat exchange between feed and return and thus allowing rapid cooldown of the panel.

Figure 2 is the cooldown characteristic of the cryopanel, where the temperatures of various points have been monitored and indicates that the liquid helium cooled surface takes approximately 2 hr to reach 20°K. The pumping speed of the cryopanel in a test chamber has beem measured for both nitrogen and neon gas and is 4000 ℓ/sec.

In addition, a long pumping test was performed, where nitrogen gas at the expected ion source usage rate (1cc/min) was flowed into the test chamber and the facility operated for 20 days, with no degradation in pumping speed. In summary, the prototype cryopanel does successfully meet the design criteria.

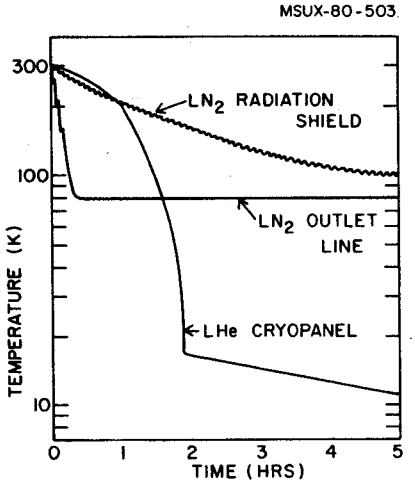

FIG. 2. The cooldown curve for the LHe cryopanel and its radiation shield are shown. The cryopanel was able to start vacuum pumping in less than 2 hrs.

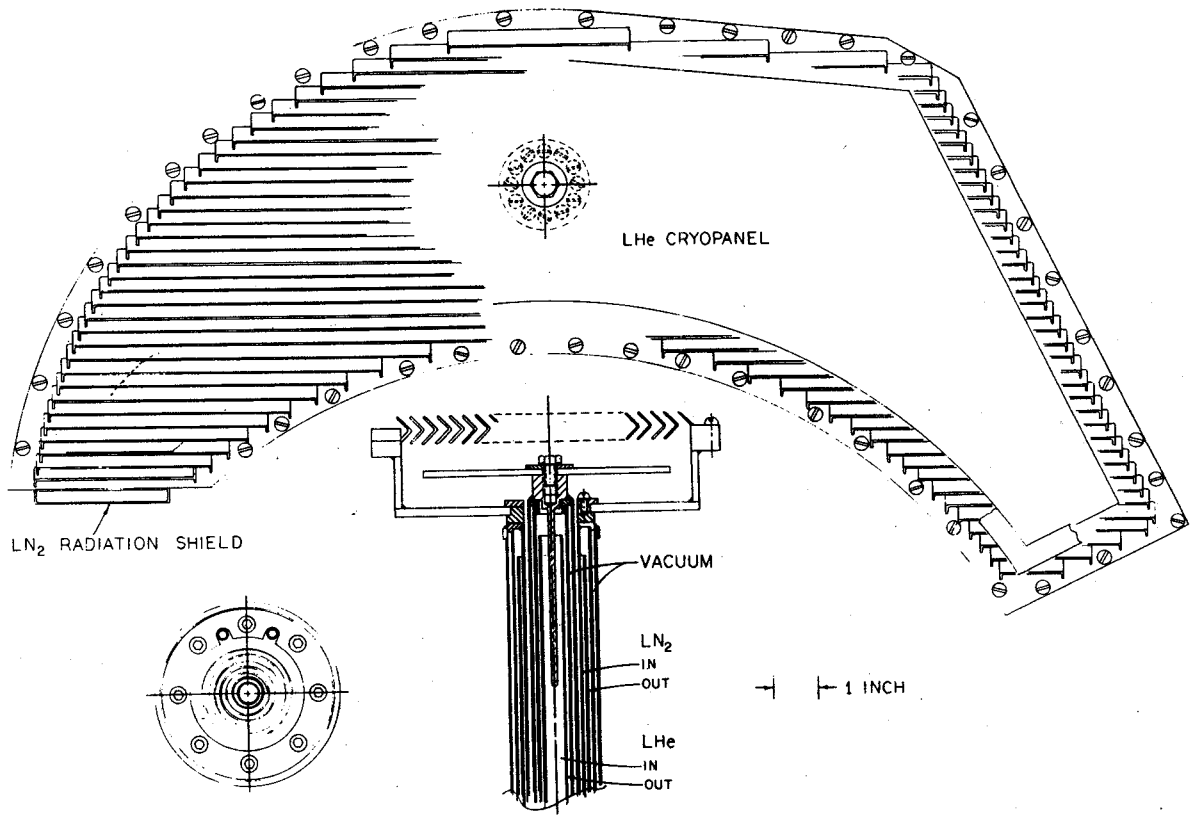

FIG. 1. Three schematic views of the cryopanel for the cyclotron are shown. The top view is the LN cooled chevron, with a cutaway view of the LHe surface. The cryopanel is shaped to fit in the rf dee. The center view shows the attachment between the cryopanel and the transfers lines that contain both LN and LHe. The bottom left view is a cross sectional view showing the many coaxial tubes used to construct the transfer line. The outer vacuum jacket is not shown.

K-500 Deflector High Voltage Tests

T. Antaya, P. Miller and D. Poe

The extraction system of the K-500 cyclotron consists of two electrostatic deflectors, eight magnetic channels, and two harmonic compensation bars. The final design features are the result of extensive calculations of the extraction beam dynamics.[1] That analysis placed the deflectors on two successive hills just prior to the entrance of the exit channel. The high voltage feedthru and the positioning mechanisms for each deflector will have to penetrate the cryostat at the median plane. The feedthru must support high voltages; for example, to extract the highest energy beam in stand-alone operation, 94 kV must be applied to the 7 mm gap between the deflector electrode and septum. Testing of the essential elements of the design is in progress. We are reporting high voltage experiments which have tested the median plane feedthru.

All of the experiments mentioned in this report were carried out in the 50 MeV cyclotron. The capability for testing deflector components in a cyclotron environment has been of great importance. The existing electrostatic deflector of that cyclotron was modified to incorporate the new features of the K-500 design, but all other cyclotron subsystems remained unchanged. The most significant difference is the small metal and ceramic coaxial high voltage feedthru. Constrained by the size of the median plane gap of the K-500 coil, the feedthru itself, not the deflector, will carry the highest electric field strengths. At 94 kV for example, the maximum deflector electric field will be 134 kV/cm. At the same time the maximum field in the feedthru will be 172.9 kV/cm, 22% higher.

The chosen high voltage feedthru design, shown in Fig. 1, consists of a coaxial arrangement of cathode and anode. The cathode, fabricated from a 0.5 inch diameter rod, is the

MSUX-80-546

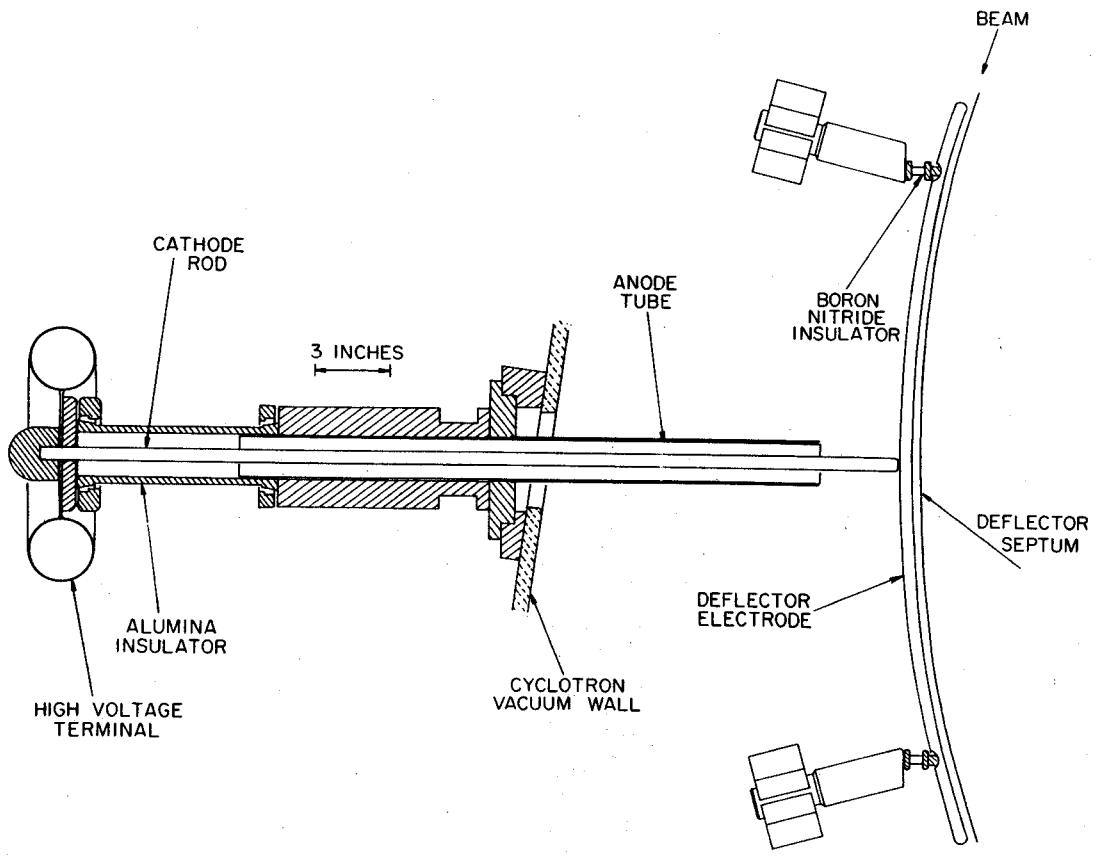

FIG. 1. Diagram of the high voltage feedthru and electrostatic deflector as installed in the 50 MeV cyclotron for the high voltage tests. The K-500 design feedthru supplies an existing deflector electrode. The length of the feedthru, measured from the high voltage terminal to the deflector electrode, is 32 inches, and will increase to 44 inches in the K-500 cyclotron. Both titanium and stainless steel anodes have been tested.

inner conductor. It is surrounded by a thin tube of 1.25 inch outside diameter which serves as the anode. This provides a very compact way to conduct the high voltage to the deflector. It also responds favorably to conditioning by moderate sparking. The 1.25 inch outside diameter of the anode represents the largest tube that can be thermally insulated from the coil with adequate clearance (the median plane gap in the superconducting coil is only two inches, and space must be provided for super-insulation). The tests done so far have concentrated on proving that this feedthru will support the required voltage and will not be destroyed by sparking. After some tests of the system with larger diameter anode tubes the objective was accomplished for two different anode materials in the required size: (1) 304 stainless steel and (2) titanium. In both cases the cathode material was stainless steel.

The stainless steel cathode - titanium anode high voltage feedthru was tested first. The 0.5 inch diameter cathode rod was polished to a highly reflective finish. The 1.25 inch O.D. (1.177 inch I.D.) titanium tube received no special surface treatment except cleaning with detergent and water. The gap between the deflector shoe and septum was set to 0.7 cm. The capacitance measured from the high voltage terminal on the feedthru to ground through the deflector was 97 pF. The 50 MeV cyclotron vacuum was generally $2\text{-}5\times10^{-5}$ torr. Initially the cyclotron main magnet field was switched off so that just electrostatic characteristics of the deflector could be studied. Charged particle beams were never present during these tests. In the first hour of operation the deflector was successfully raised to 100 kV. At 100 kV, the extraction field is 142.9 kV/cm. This is 7% higher than the maximum field that will be required for extraction of K-500 beams. However, both the sparking rate and dark current were unacceptably high. The dark current initially 2 μA at 100 kV, grew to over 40 μA in the first 5 minutes as the result of sparking. This is undesireable because a large, fluctuating dark current destabilizes the deflector voltage. The high voltage lead from the power supply to the deflector had a 1.1 MΩ resistance to limit the short circuit current during sparks. Dark current causes a voltage drop across that resistor. Fortunately through electrostatic conditioning it is possible to reduce the dark current to the point where even more resistance can be tolerated. After running the deflector for several days at voltages above 90 kV, the dark current dropped to less than 1 μA and the sparking rate nearly to zero.

Even for a conditioned deflector the dark current increases with the applied voltage. In Fig. 2 the variation of the dark current with deflector voltage is shown in several situations for this deflector arrangement. Curve (1) is the dark current history of the deflector after electrostatic conditioning. The dark current goes above 1 μA only for voltages greater than 100 kV. The highest voltaged attained by the deflector in this configuration was 114.29 kV. This corresponds to a 163.3 kV/cm extraction field. After a period of running at voltages above 100 kV we found that the sparking rate at lower voltages (90-100 kV) was negligible. Once conditioned, low sparking rates appeared to be easily achievable after a short warmup period.

MSUX-80-547

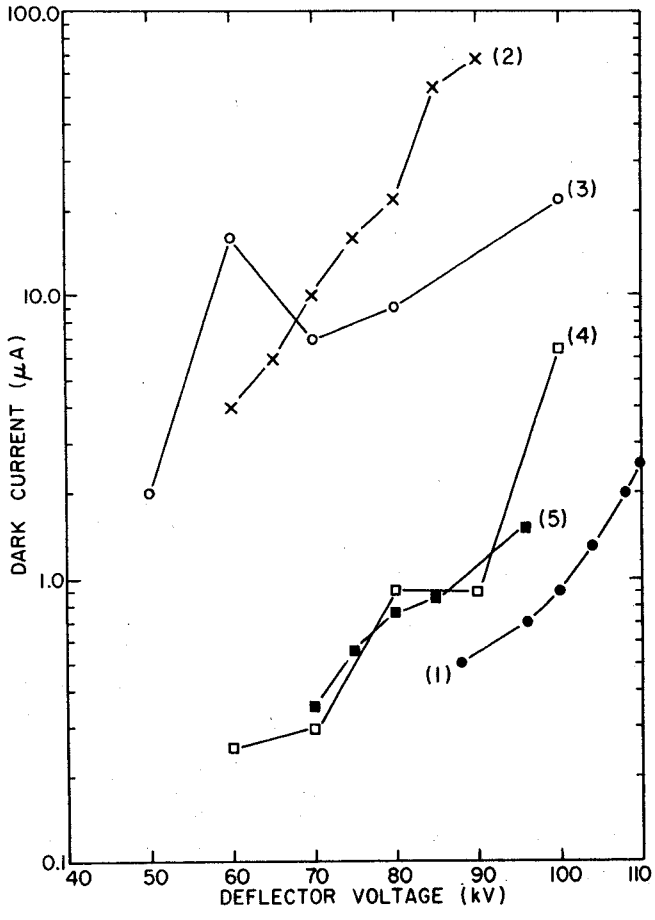

FIG. 2. The dark current, measured from the high voltage terminal to ground through the deflector, with a 1.75 inch O.D. titanium liner installed in the feedthru, as plotted during a sequence of conditioning experiments:
(1) after extensive electrostatic conditioning at voltages above 90 kV
(2) after sparking damage has occurred in a 10 KG cyclotron magnetic field
(3) liner polished to removed the sparking pits formed in case (2)
(4) additional electrostatic conditioning has lowered the dark current substantially
(5) raising the value of the high voltage current limiting resistance from 1.1 MΩ to 5.2 MΩ results in low dark current in the presence of a 10 kG magnetic field.

The initial tests confirmed that the K-500 high voltage feedthru design could support very high static voltages. Next we tested the deflector in the presence of the cyclotron magnetic field. In Fig. 3 the location of the deflector is shown in relation to the average magnetic field profile. The high voltage feedthru passes through the magnet fringe field. This situation will also occur in the K-500 cyclotron, but the field gradient will be larger.

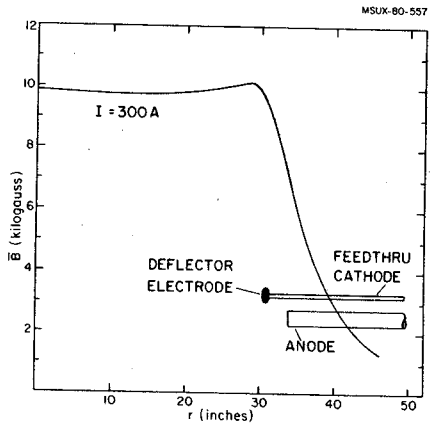

FIG. 3. Azimuthal average value of the axial magnetic field component for a 300 amp excitation of the main coils in the 50 MeV cyclotron. The high field ends of the deflector electrode and feedthru elements are shown relative to the magnet fringe field.

High voltage sparking in a magnetic field is a more difficult problem. Sparks follow the magnetic field lines and strike the anode with a higher energy density. Recall that curve (1) of Fig. 2 showed the dark current of the deflector with the 1.25 inch titanium anode after many days of operation without magnetic field. Such a low dark current as this (1 μA) resulted in stable deflector operation (steady voltage, few sparks). The sparks that occurred at low dark current took less than 4 μsec to discharge and extinquish. Continuous arcing was never observed. When the cyclotron magnet was turned on the situation became suddenly worse. In curve (2) of Fig. 2 the dark current is plotted after the conditioned system was raised to high voltage in the presence of a 10 kGauss magnetic field. The dark current at 90 kV was over 100 times larger than in curve (1). Since the sparking rate was typically a few sparks per minute for dark currents over 10 μA, excessive beam loss would result if an operating deflector had such a sparking rate. Continuous arcing from the feedthru cathode to the inside surface of the anode at the end in the high magnetic field was observed when the voltage reached 100 kV. Subsequently several attempts were made to raise the deflector to 100 kV, but each time at about 90 kV the continuous arcing would commence. Disassembly revealed substantial pitting of the inside surface of the anode, along the top and bottom of the end in the high magnetic field. Vaporized metal had condensed on the cathode at corresponding locations. There was no evidence of deleterious sparking on any other deflector surface. Hence the high dark current in curve (2) must be attributed to the damaged anode. It was polished using a succession of aluminum oxide grits to remove the spark pits. The stainless steel cathode was buffed to remove the deposited metal. Curve (3) in Fig. 2 shows the dark current with the newly polished titanium liner in place. Substantial lowering of the dark current at high voltage has occurred through the removal of the sparking damage. In addition, the dark current was reduced even further through electrostatic conditioning. Figure 4 shows the decrease in the dark current of the repolished liner during the first 6 hour period at 90 kV. After about 20 hours at voltages above 90 kV, the deflector did condition down to curve (4) of Fig. 2. At that time the deflector voltage was again raised in the 10 kG field. At 97 kV the continuous arcing returned. The sparks that were forming had sufficient energy to melt the titanium liner, setting up a self-sustaining short circuit and locally producing pits. We then increased the resistance between the power supply and deflector from 1.1 MΩ to 5.2 MΩ to reduce the maximum short circuit current. Observations of deflector sparks then showed that once again their duration was 4μsec or less, and self-extinguishing. With this new high voltage lead resistance in place the deflector voltage was raised once more. The combination of slow voltage adjustment to avoid sparks and increased circuit resistance was used to successfully condition the deflector to high voltage in the strong magnetic field. Curve (5) in Fig. 2 shows the dark current of the deflector with the SS-Ti feedthru after 18 hours at voltages between 90 and 94 kV in the magnetic field. At 94 kV the deflector electric field just exceeds the 133 kV/cm field required for the extraction of the highest energy beams in stand-alone operation of the K-500 cyclotron. Additional testing showed that the system could go as high as 100 kV without difficulty.

Based on the experience obtained operating the 50 MeV cyclotron deflector with the SS-Ti feedthru, tests of an all stainless steel feedthru were performed. The outside of the stainless steel anode was still 1.25 inches, but the wall thickness changed to 0.035 inches from the 0.042 inch the titanium anode. The new anode received no special polishing treatment.

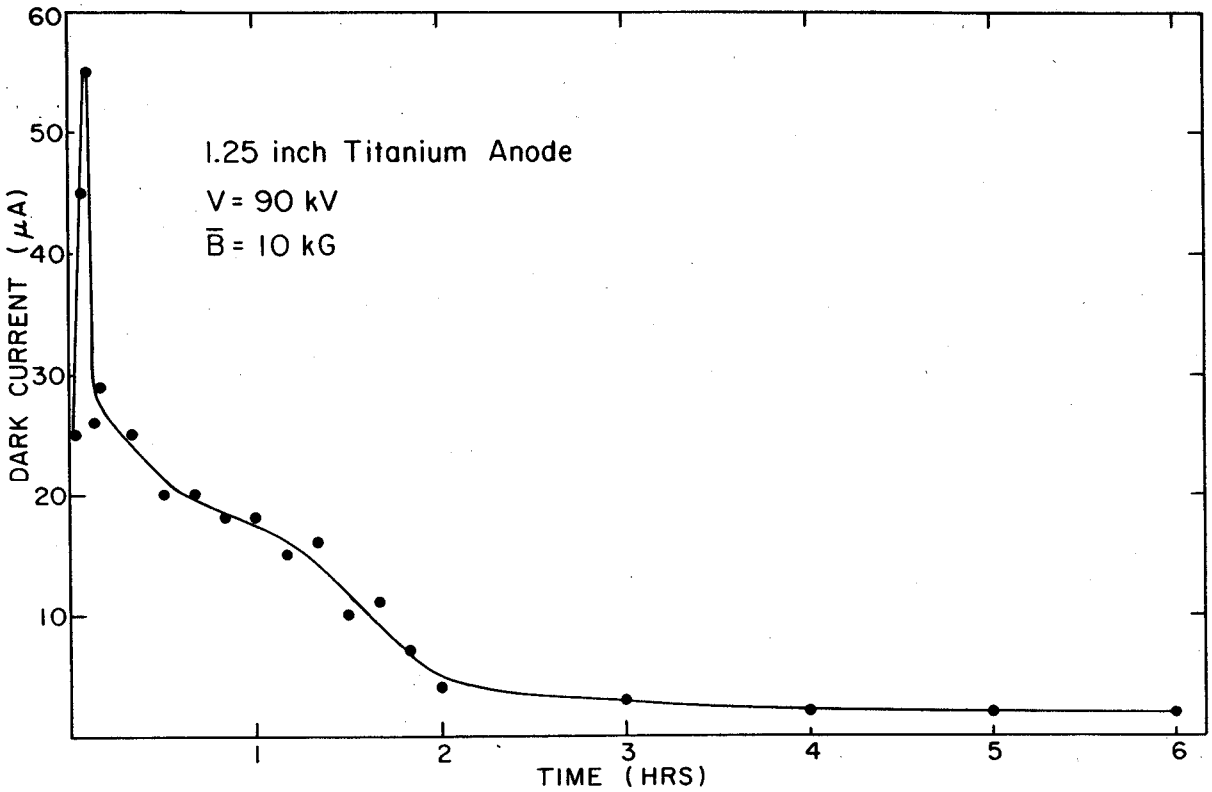

FIG. 4. Dark current conditioning curve with the repolished 1.25 inch titanium anode installed in the high voltage feedthru.

In the first test the voltage was raised slowly to 85 kV. The dark current at 85 kV was 4 μA and the initial spark rate about 2 sparks per minute. The voltage was held at 85 kV for 16 hours and the dark current conditioned to 1 μA with less than one spark per ten minute interval. Eventually the voltage was raised to 102.1 kV. The dark current versus voltage was remarkably low for the new system, as shown in curve (1) in Fig. 5. This possibly reflects the fact that the stainless steel tube was manufactured with smoother inner surface than the titanium tube. After only 40 hours of electrostatic conditioning, the deflector was raised from zero to 90.1 kV in 1.5 minutes in a 6 kGauss magnetic field, and it was held continuously above 90 kV for the next 4 days. After that run inspection of the feedthru showed no evidence of spark pitting. The final measured dark current for this system is shown in curve (2) of Fig. 5.

The basic high voltage feedthru design is adequate to support the electric fields required for extraction of beams from the K-500 cyclotron. It appears that the all stainless steel feedthru withstands sparking better than the SS (cathode) - Ti (anode) feedthru. However, all of the basic studies were performed on the latter system, which clearly degraded its ultimate performance. Comparison testing of these two systems will be necessary to quantify the relative merits of each, but both are evidently viable. The deflector dark current was an effective guide to high voltage conditioning; dark currents under 10 μA at voltages above 90 kV reduce sparking and deflector voltage fluctuations substantially. Increasing the high voltage lead resistance decreases sparking damage. No changes in performance are expected in the K500 environment. The total capacitance will increase moderately due to the longer coax line and smaller axial vacuum gap required at the deflector. Likewise, the increase in the magnetic field to 50 kg is not expected to bring any new difficulties. Additional tests of the prototype deflector are planned, with attention to be focused on the support insulators for the deflector electrode.

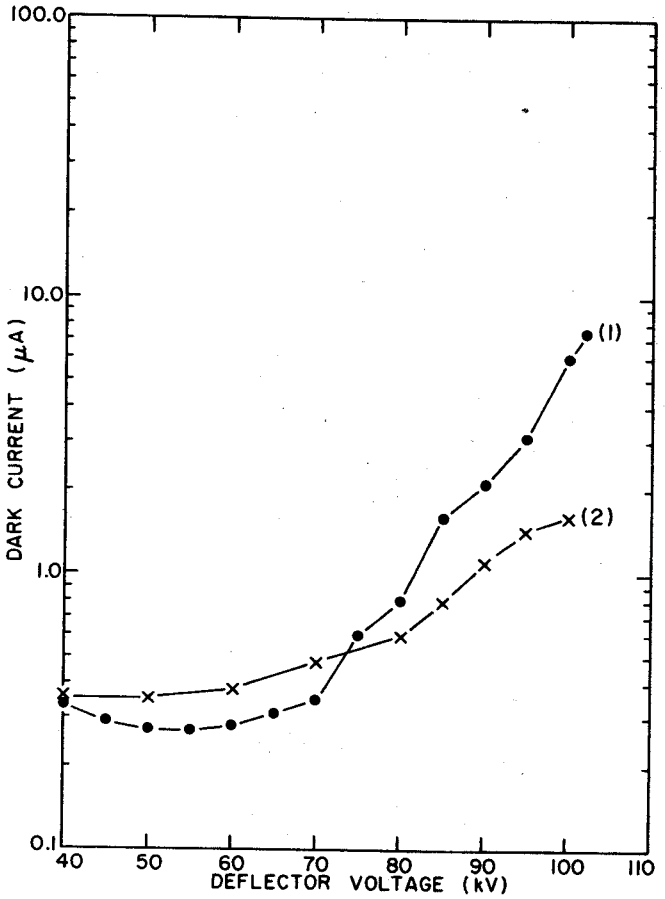

FIG. 5. The deflector dark current with a 1.25 inch stainless steel anode in the high voltage feedthru:
(1) after 20 hours of operation above 85 kV
(2) after additional conditioning in a 10 kG magnetic field.

1. E. Fabrici, D. Johnson, F.G. Resmini, The Extraction System for the K-500 Cyclotron at MSU. MSUCP-33, June 1980.

First Harmonic

During the past year, we have been improving the design of the first harmonic central region for the K500 superconducting cyclotron. Our new design resembles closely the one reported earlier,[1] where we have modified the puller region to allow for a larger distance between the puller posts and the second dee post.

In the first harmonic operation, the phase difference between dee voltages is 120 RF degrees. With a dee voltage of 100 kV the maximum potential difference between dees is then 100 $\sqrt{3}$ kV. Since the dummy dee comprised between dees 1 and 2 has been cut back (see Fig. 1), it does not shield one dee from the other. Under our assumption of limiting the maximum electric field in the central region to 100 kV/cm to avoid sparking, the closest distance between dees should be at least 18 mm.

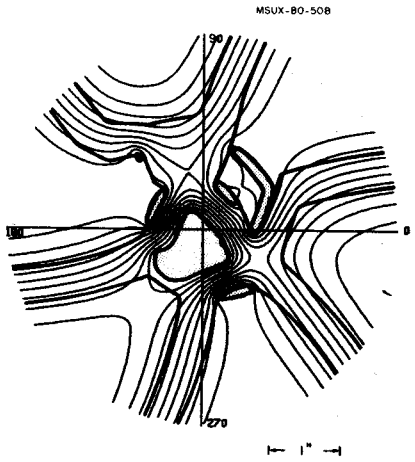

FIG. 1. Central region of the K500 Cyclotron for first harmonic operation. The dees are indicated by heavy lines, and the posts by dotted regions. The equipotentials shown are obtained when all three dees are excited with the same voltage.

Some modifications had to be made to allow the ion source to rotate $\pm 5^{\circ}$. Figure 1 shows the equipotential lines when all three dees have the same voltage. We must note this will never be the case in first harmonic operation (it corresponds to the third harmonic case), but it identifies clearly the posts and gaps.

We have used as test particles in our studies the following particles:

a) Q/A = 0.322, Bo = 45.5 kG, E ≃ 50 MeV/A, located on the focusing limit of the operating diagram.

b) Q/A = 0.5, Bo = 36 kG, E ≃ 80 MeV/A, also on the focusing limit.

c) Q/A = 0.286, Bo = 44.7, E ≃ 38 MeV/A, located on the bending limit.

We concentrated our efforts on the high turn number particles because they are the most difficult cases, having the smallest radius of curvature, and consequently the dee posts are real obstacles in their paths. The orbits were computed with the Cyclone code using electric fields derived from the potential maps measured with an electrolytic tank. Figure 2 shows three orbits for the Q/A = 0.322 particle where the starting times are 20, 30, and 40° before reaching the peak voltage between source and puller. The center ray is perfectly centered after twenty turns (within a few mils), and the average phase in the first turn is 25°. The phase behavior is shown in Fig. 3 where we can see that after twenty turns the phase is just 4°. The rays that start within ± 10 RF degrees of the central ray have centering errors of less than 45 mils and clear the posts, determining a phase acceptance of $\pm 10^{\circ}$.

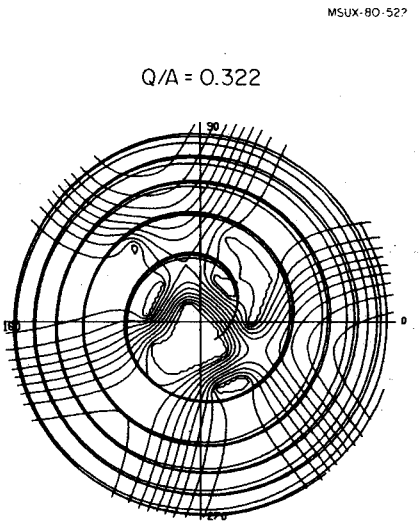

FIG. 2. Orbits of the Q/A = 0.322 particle in the field B_o = 45.5 kG. The starting times are 20, 30 and 40 RF degrees before peak voltage between ion source and puller.

Starting the Q/A = 0.5 particle at the same ion source position that we found optimizing the centering of the 0.322 particle gives an orbit centered within 15 mils, with an average phase on the first turn of 23°, and similar phase acceptance to the previous case.

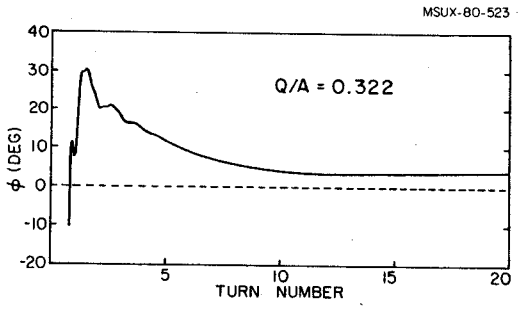

FIG. 3. Phase history of the Q/A = 0.322 particle in the field B_0 = 45.5 kG. The starting time is 30 RF degrees before peak voltage.

The Q/A = 0.288 particle corresponds to a relatively low turn number case (about 450 vs. 540 for the other two particles). Starting at the same ion source position, the centering error was 30 mils and the average phase in the first turn approximately 21°.

Anticipating possible difficulties in obtaining 100 kV due to sparking in the center of the machine, we have determined that the minimum dee voltage that can be used with this central region geometry is approximately 90 kV. Below this voltage it is difficult to clear the post in the third dee without lowering the magnetic field and therefore decreasing the final energy.

Second and Higher Harmonics

In our study of the h=2 central region, we found that one of the major difficulties was the excessively long transit time between source and puller.

The starting time $\tau_o = -130^\circ (=\omega_{RF}\, t_o)$ was picked as a compromise between maximum energy gain and maximum intensity. Our desire is that the particle reaches the puller for $t \approx 0^\circ$ and not later, otherwise it will lose energy. (The voltage reverses sign for τ=0).

The first idea was to decrease the dee voltage from 100 kV to 80 kV keeping the electric field constant in the source to puller region by decreasing the size by 0.80. This certainly brought the crossing time down to what we wanted for the $^{14}N^{3+}$ test particle. We decided then to do a survey of transit times for different particles, voltages, and harmonics.

From the orbit plots obtained in this survey, it was evident, especially for higher harmonics, that the orbits do not depart too much from a straight line. We decided then to try a simple model of the source to puller motion, considering just a uniform sinusoidally varying electric field and neglecting the effect of the magnet field.

We now introduce Reiser's parameter:

$$\chi = \frac{q}{m}\,\frac{d^2B^2}{V_o}$$

where d is the source to puller distance. Then,

$$\Delta\tau = \tau - \tau_o \simeq \frac{\sin\tau_o - \tau_o}{1-\cos\tau_o} + \frac{h^2\chi}{1-\cos\tau_o}$$

We see that the transit time $\Delta\tau$ increases linearly with χ, i.e., with q/m keeping the other parameters constant. A comparison of this simple relation with the transit times obtained from the Cyclone code gives a good agreement. For each harmonic we have a starting τ_o, and fixing τ_{final}=0 we obtain a relation

$$\chi = c\ (h)$$

or

$$\frac{Q}{A}\,\frac{B^2 d}{F} = c\ (h).$$

In our studies we keep the electric field F fixed and scale the voltage V_o = 100.s kV, obtaining:

$$\frac{Q}{A}\,B^2\, s = c\ (h).$$

We can then represent in the operating diagram B vs. Q/A of the K=500 cyclotron the maximum voltages V_o that can be used with given B and Q/A to have $\tau_{final} \simeq 0$.

Up to now, we have considered only the limitations imposed on the dee voltage by the transit time between source and puller. But we have to take into account the maximum and minimum turn number limits. From the maximum acceptable phase swing we obtain

$$\text{Max } N_t = \frac{1000}{h}$$

Due to the limitation that the ion source must fit inside the central magnet hole, we have

$$\text{Min } N_t = 100.$$

These numbers are very approximate now, but they give us an idea of the range of associated voltages that we have to use. If s is the scaling factor for the voltage, we then have:

(a) $s \le C_1 \frac{1}{\nu_o{}^2}\ \frac{Q}{A}$ to have $\tau_{final} \le 0$

(b) $s \le C_2 \frac{\nu_o{}^2}{(Q/A)}$ to have $n_t \ge N_{tmin}$

(c) $s \ge C_2 \frac{\nu_o{}^2}{(Q/A)}$ to have $n_t \le N_{t\,max}$

Figure 4 shows the range of scaling factors s allowed with each $\frac{\nu_o{}^2}{Q/A}$.

In the interval (1) the maximum voltage is limited by the minimum number of turns, while in the interval (2) it is limited by the transit time. In the interval (3) it is not possible to satisfy all these conditions. In the

lower harmonics the maximum turn number limitation might not exist and there is no interval (3), but in the higher harmonics there is.

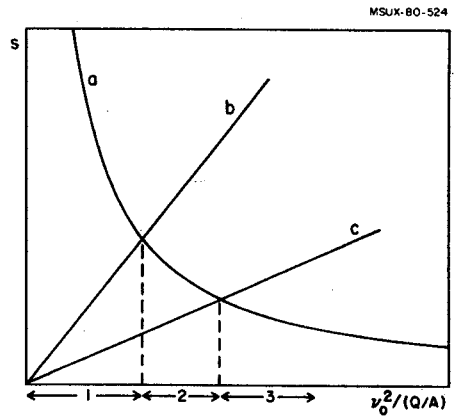

FIG. 4. Limitations on the dee voltage, s = V(kV)/100. The allowed region is below curve a to obtain $\tau \leq 0$, below curve b to have the turn number larger than the minimum, and above curve c to obtain a turn number lower than the maximum.

Vertical Motion

The Cyclone code allows us to study the axial motion of particles using an electric field correct to first order in z. This electric field is calculated from the Laplacian of the electric potential measured in the electrolytic tank.[2]

Since the equations of motion are linear, it is enough to determine two independent solutions that start with different z, p_z. Any orbit with arbitrary initial conditions can be generated by linear superposition of these two basic solutions. This fact allows us to find the envelope of a beam in a simple way when we know the axial phase space occupied by it at the center of the machine.

To determine the vertical acceptance in the central region, we assume that the beam occupies an ellipse in the z, p_z phase spaces and follow the evolution of this ellipse for forty turns using the transfer matrix method. The ellipse has arbitrary eccentricity and tilt. We determine them in such a way as to obtain the maximum area in phase space with the limitation that the z envelope is always smaller than a given maximum amplitude. In our case we took the maximum height of the beam to be 0.5 inch. Figure 5 shows the envelope for the 80 MeV/A, Q/A = 0.5 particle, that gives an acceptance of 264 π mm mrad at T=16 keV/nucleon.

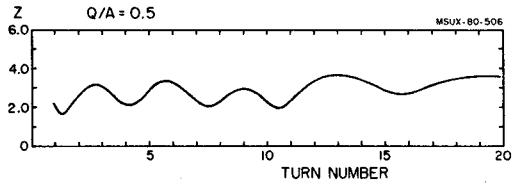

FIG. 5. Z-envelope for the Q/A = 0.5 particle in the field B_o = 36 kG, with arbitrary units in the Z axis. It should be scaled so that Z = 3.8 in the figure corresponds to 0.25 inch.

1. E. Liukkonen and T. Antaya, Cyclotron Laboratory, M.S.U., Annual Report 1978-1979, p. 107.
2. M.M. Gordon and E. Liukkonen, Cyclotron Laboratory, M.S.U., Annual Report 1978-1979, p. 123.

Study of the Forces on the Aluminum Heat Shield Due to Eddy Currents

F. Marti and M. Gordon

The nitrogen cooled shield of the K500 MeV cyclotron, called for brevity the nitrogen shield, was opened in January 1980 to take out the superconducting coil. It was then obvious that the exterior circular cylinder had collapsed toward the center, resulting in the flattening of the lateral face into a pretty regular polygon.

Some of the faces were firmly touching the superinsulation and pressing it to the helium can. Since this is undesirable from the heat transmission point of view, it was decided to study the different situations that could have produced the bucking of the outer cylinder. The inner cylinder did not show any sign of deformation.

We decided to investigate three situations that could have produced large eddy currents in the aluminum shield: a) normal dump, b) accident which occurred in October 1977 when one of the horizontal links broke, and c) accident which occurred on September 19, 1977 when the dump resistor burned out. Figure 1 shows the dimensions of the nitrogen shield.

MSUX-80-507

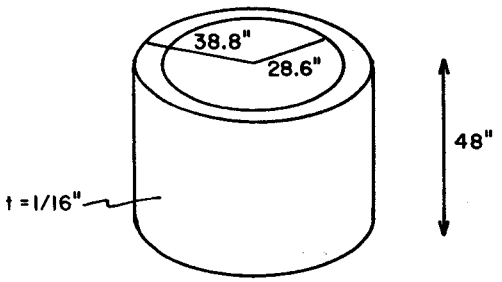

FIG. 1. Dimensions of the nitrogen cooled aluminum shield for the K500 superconducting coil.

Normal Dump

During a normal dump we can assume that the magnetic flux enclosed by any closed curve decreases as

$$\frac{d\phi}{dt} = -\lambda\phi, \qquad \text{with } \lambda \approx \frac{1}{150s}$$

Let's consider a cross section perpendicular to the axis of the aluminum shield, and call C the integration path along that cross section. By Faraday's law

$$\int_C \vec{E}\,\vec{dl} = -\frac{d}{dt}\int \vec{A}\,\vec{dl}$$

therefore,

$$E_\theta = -\frac{\partial A_\theta}{\partial t} = \lambda A_\theta$$

The force per unit volume is

$$\frac{\vec{dF}}{dv} = \vec{J} \times \vec{B}, \qquad \text{with } \vec{J} = \sigma\vec{E}$$

The pressure on the metal surfaces will then be

$$p = \frac{df}{ds} = |JxB|\,t = \sigma E_\theta B_x t,$$

where t=thickness of aluminum sheet.

If we consider the lateral faces, the pressure will be obtained by taking $B_x = B_z$. If, instead, we are considering the horizontal faces we must take $B_x = B_r$.

It must be noted that by Lenz's law the eddy currents induced in the aluminum will try to counteract the decrease in field and will then have the same direction as the coil current. The forces on the currents will be attractive, indicating that the pressures on the different faces will be toward the interior of the aluminum can. That means that the exterior cylinder will tend to collapse, while the inner one will tend to expand. Once the collapse starts the flux will decrease even more due to the smaller area, increasing the pressure toward the center. The equilibrium is unstable. On the contrary, the equilibrium of the inner cylinder is stable since the pressure tends to increase the radius.

The forces on the top and bottom plates will be very small due to the holes that exist on those two plates, increasing enormously the resistance of the circuit.

In Figures 2a, b we show the electric field E in V/m and the pressure in psi for the inner cylinder (r=28.6 in) and the outer cylinder (r=38.8), respectively.

The critical collapsing pressure is given by:[1]

$$P_c = KE\,(\tfrac{t}{D})^3 \quad \text{psi}$$

In our case L/R=1.26, D/t=1240 giving:

a) Radial external pressure with simply supported edges

$$K \approx 200 \qquad P_c \approx 1 \text{ psi}$$

b) Radial and end external pressure with simply supported edges

$$K \approx 120, \qquad P_c \approx 0.6 \text{ psi}$$

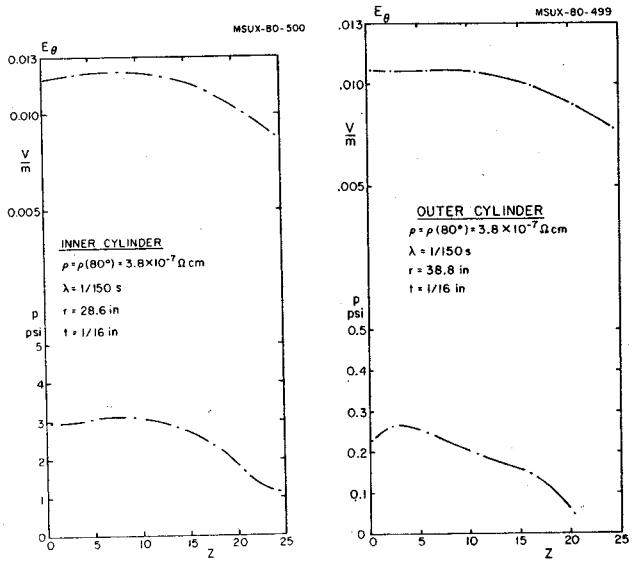

FIG. 2. (a) Electric field in V/m and pressure in psi for the inner cylinder in the nitrogen shield during a normal dump.
(b) Idem for the outer cylinder.

We note that according to the graphs given in Mark's Handbook the number of faces a cylinder with the dimensions of ours would collapse into is about 11 or 12. This number agrees well with the observed number of faces.

As we can see from Fig. 2b, the maximum pressure on the outer cylinder in a normal dump with λ= 1/150s is only 0.27 psi.

There is also a vertical force on the lateral faces produced by the interaction of the eddy currents with the radial component of the magnetic field. This force is small compared to the axial load capable of producing buckling by itself that we estimated as[2]

$$F_c = 9x2\pi Et^2(\frac{t}{R})^{0.6} = 4.66x10^4 \text{ lb}$$

The force per square inch in our exterior cylinder is given in the following table. The plus sign indicates force toward the median plane (z=0); minus away from it.

z	0	5	10	15	20	25
F_z(psi)	0	-0.06	0.193	0.62	0.98	0.74

Broken link accident

When the horizontal link broke, the coil can moved approximatley 1 cm in a very short time, producing a rapid flux decrease inside the aluminum shield. If we neglect the self inductance of the aluminum cylinder, we can estimate in what time the displacement must have occurred to produce the critical pressure on the cylinder wall. Our estimate is approximately 2 ms. This is an extremely short time and the force necessary to produce this sudden displacement is excessively high. If we consider the self inductance, the result makes this accident even more unlikely to produce the collapse of the nitrogen shield.

Dump resistor accident

As arcing was observed during this accident, we know that the voltage in the coil was higher than normal, indicating a rapidly changing current. Recalling the results obtained in the study of the normal dump, we observe that a transient with a time constant of 40 seconds or smaller would be enough to produce the critical pressure necessary for buckling the can.

Magnetic field data

The magnetic field data necessary for our computations were obtained from a special run of the TRIM code. The current was 700 A in both coils and there was a center plug. We must note that besides giving the $B_r B_z$ components and its derivatives the TRIM code also prints the values of rA , that is, the quantity needed to compute the flux.

Conclusion

Our study showed that:

1) The pressure produced in a normal dump is not large enough to buckle the can. The time constant of current decay should be at least four times smaller than the observed one for the pressure to reach the critical buckling value.

2) In the broken link accident, our estimate of the force on the coil necessary to produce a change in positon fast enough to generate eddy currents capable of buckling the can is 5000 tons. This value looks excessively high.

3) We conclude that the flattening probably occurred during the accident that burned the dump resistor.

---

1. C.W. MacGregor, in Mark's Mechanical Engineers Handbook 6th Edition (McGraw-Hill, New York, 1958) p. 5-63.
2. V.I. Weingarten, E.J. Morgan and P. Seide, AIAA 3, 500 (1965).

Cryolines

H. Laumer, M. Mallory, D. Lawton, J. Ottarson and A. Gavalya

The K=800 and K=500 superconducting cyclotron system with possibly many superconducting beam handling and experimental equipment magnets will require a sophisticated cryogen distribution network. To gain experience in controlling and understanding the behavior of such a network a prototype system was designed for the K=500 superconducting cyclotron.

The design of a cryogen distribution system has to address mainly three areas of potential system failure.

a) The system must be so constructed that it does not represent an excessive heat load.

b) The system must be able to survive the mechanical stresses occasioned by materials contracting as they are cooled to cryogenic temperatures.

c) The system must be able to carry the peak mass flow required by components, this means the design is such that pressure drops in the piping do not limit the mass flow.

The helium distribution system can easily become a major component of the heat load of the liquid helium (LHe) refrigerator. A number of design techniques are incorporated in the prototype system to reduce energy influx. All cold boxes which house piping network hardware, bayonets, control and relieve valves, also incorporate a liquid nitrogen (LN_2) cooled shield. All LHe lines in the boxes are wrapped with superinsulation (multiple layers of aluminized mylar and Dexter paper-glass insulation). The cold box is under vacuum. Long LHe transfer lines have LN_2 cooled heat shields with superinsulation in the vacuum space between heat shield and LHe line. Valve stems, which represent a comparatively large heat load, have LN_2 clamps to intercept a large part of the energy. Other sources of thermal energy are safety pop off valves for pressure relief and bayonet couplings incorporated for convenience in assembly, testing, and any necessary future modifications of the system. The present design relies on the poor thermal conduction down a 0.89 mm wall thickness stainless steel tube to limit heat conduction from these sources; LN_2 clamps are easily incorporated on the stems of the relieve valves.

Mechanical stresses due to cooldown contractions of longer pipes are minimized by using flex hose. The construction is such that the stress on the flex hose is perpendicular to its axis of symmetry. For efficient heat shielding, tubing carrying LHe runs inside of LN_2 carrying pipes; this leads to some intricate structures for stress relief. All components carrying cryogenic liquids and gases are made of stainless steel. All joints are welded and before leak checking with a helium mass spectrometer, they are cold shocked with LN_2. Any component system which will handle LHe or LN_2 is tested by flowing liquid nitrogen through the assembly. It is expected this test will ferret out any problems before the system is completely assembled.

The cryogenic system requirements for fluid transport are varied. For example, in cooling down the magnet cyrostat, gas from the refrigerator at a relatively warm temperature of 100 K is initially returned at 300 K. Eventually gas near 5 K delivered to the magnet is returned below 100 K from the magnet. Finally liquid fills the cryostat volume and the cold boiloff gas is returned to the refrigerator and is used in precooling the compressed helium gas. The physical dimensions of the liquid transfer line have a large impact on its heat load, so a small liquid feed line is advantageous. This line can then not be used to supply gas in the cooldown process because it would represent too high an impedance which would cut the mass flow to an unacceptably low level.

Cryogenic streams of single phase liquid or single phase gas are much more easily characterized than two-phase fluids, and generally the single phase fluid flows with less resistance. The turbulent conditions in two-phase flow are also expected to present a more difficult problem for automatic operation because temperature and pressure sensor response as well as non-linear behavior of the fluid in going through control valves can more easily lead to hunting by the control system. One technique to insure single-phase liquid flow and hence improve mass flow characteristics is to subcool the feed line. The K=500 cyclotron cryogenic distribution system incorporates a LHe feed line at 1.8 atmospheres running inside a 1.2 atmosphere subcooling line which returns part of the 1.8 atmosphere helium stream to the refrigerator-liquefier.

The cryogenic system thus incorporates:

a) a main branch subcooled LHe feed line,

b) side branches feeding components which initially are the magnet cryostat and the cryopanels for the cyclotron vacuum system,

c) cooldown gas feed and return lines as well as lines for returning the boil off gas from the LHe pools of these two devices to the appropriate temperature tap in the refrigerator heat exchanger,

d) LN_2 feed lines for heat shields and for cooling compressed helium in the refrigerator-liquefier,

e) nitrogen gas vent lines for the nitrogen boil off gas generated.

It is apparent that the characteristics of the fluids piped cover a wide range in temperature, viscosity, density, and mass flow. The system has been designed so that at least in single phase flow regimes all pressure drops through the network not associated with control valves are below 1 PSI. Table 1 summerizes a few expected flow regimes through circular pipes. The table gives the maximum pipe length allowed for which the mass flow required through the pipe of diameter D will cause a fluid pressure drop of 1 PSI.

The cryosystem will essentially have two modes of operation, transient, for equipment cooldown, and steady state, for maintaining LHe levels. The transient phase of the operation will be conducted manually and will usually require close supervision. The steady state phase will be controlled automatically. Signals from silicon diode temperature sensors and from differential pressure sensing devices will be interpreted by decision making modules which will control pneumatic transducers which in turn operate fluid control valves to maintain desired liquid levels or pressures.

The construction of the cryodistribution system is presently underway. One of three cold boxes which house control valves has been completed. Most hardware for the second cold box is completed and awaits assembly.

Table 1.

FLOW REGIME	FLUID TYPE	MASS FLOW ($\frac{g}{s}$)	FLUID PRESSURE (atm)	FLUID TEMP (K)	FLUID VISCOSITY ($\frac{kg}{ms}$)	FLUID DENSITY ($\frac{kg}{m3}$)	PIPE DIAMETER (in)	ΔL for ΔP=1PSI (m)
1	He	15	1.2	300	$1.99*10^{-5}$	0.195	2.0	97
2	He	3	1.2	100	$9.78*10^{-6}$	0.584	0.75	55
3	He	2.9	1.8	4.9	$2.73*10^{-6}$	106	0.25	68
4	He	2.9	1.2	4.4	$1.34*10^{-6}$	20.5	0.5	450
5	N_2	23.6	1	300	$1.80*10^{-4}$	1.25	2.0	170
6	N_2	51	1	77	$1.58*10^{-3}$	808	0.652	126

The calculations are appropriate for:

1. warm He gas returned to compressor or He gas used to cool down the magnet from 300°K;
2. cold He gas returned to refrigerator;
3. the sub-cooled liquid He line;
4. the He bath for the subcooled line; actually L is 200 if the inside line is 0.25 in. diameter;
5. the N_2 boil off gas during magnet cooldown;
6. the liquid N_2 supply line assuming a maximum flow rate of 1 gal/min.

Superconducting Magnet Cryogenic Operation

M. Mallory, H. Laumer and D. Poe

Details of previous cryogenic operations have been reported in other annual reports; a short summary of the latest results are reported below.

Measurement of Median Plane Heat Load

In the first assembly of the magnet cryostat, penetrations through the median plane were built with the intent that these would simulate the heat load of the beam extraction system. The completed design of the beam extraction system has about a magnitude increase in surface area over the test penetrations and it was decided to measure the heat load of the test penetrations. Assuming good convection and heat exchange at the stainless steel to air interface, the heat load of the test penetrations was calculated to be 0.12ℓ/hr. The heat load becomes negligible when the penetrations are evacuated. The average boil off rate at the median plane with the penetrations evacuated was measured to be 1.75 ± 0.25ℓ/hr. For the case when air was allowed to freely circulate through the penetrations a boil off rate of 2.18 ± 0.25ℓ/hr was determined. Considering the precision of the measurement the agreement with the calculation is reasonable.

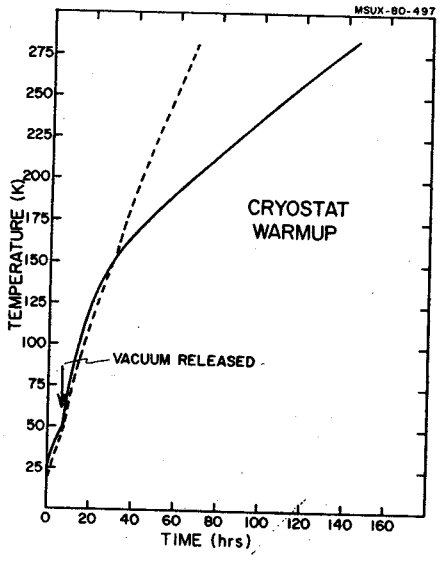

FIG. 1. Two regimes for warming up the magnet cryostat to room temperature are compared. The dashed line represents warmup with temperature controlled gas using the helium refrigerator. The solid line represents a passive mode where the insulating vacuum of the cryostat is broken at the temperature indicated.

Cryostat Warm Up

The initial method used to warm up the magnet cryostat has been to let dry nitrogen gas into the vacuum jacket after the coil warms to 40° K. This technique takes approximately 130 hrs. It also causes water to condense on the vacuum jacket, which then comes into contact with the magnet iron, thereby causing rust.

The method now used requires running the liquid helium refrigerator. Namely, gas at 100° K warmer than the coldest coil temperature sensor reading is delivered to the cryostat. The gas returns through a room temperature connection. Figure 1 compares the warm up time for the two methods. The method using the refrigerator (maintaining the cryostat vacuum) takes approximately 60 hrs.

Cryostat Helium Leak

We have previously reported a method of finding ultra small leaks in the magnet cryostat. This previous method is based on passing very cold helium gas through the suspected leak

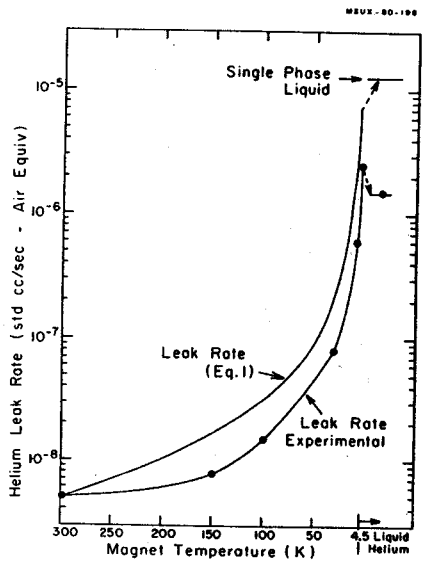

FIG. 2. The measured increase in the helium concentration in the cryostat vacuum jacket as the superconducting coil is cooled to liquid helium temperature is shown. A theoretical leak rate curve as a function of temperature is also shown and compares favorably with experimental results. The theoretical single phase liquid leak rate is larger than the gaseous leak rate, whereas the experimental leak rate is found to drop below the gaseous leak rate when the cryostat is full of liquid helium.

area. The bottom portion of the cryostat cannot be tested by this method.

The helium leakage into the cryostat has been found to increase as the coil is cooled (Fig. 2) and indicates that a helium leak was still present in the cryostat. It was found that the helium leakage would change as the cryostat was filled with (or emptied of) liquid helium. Correlating the helium leakage rate with the liquid helium height in the cryostat has allowed the vertical location of the leakage channel to be found. Figure 3 shows the helium leak rate change as liquid helium boils from the cryostat. Upon disassembly of the cryostat to install the beam extraction penetrations, a leak was located in the median plane of the cryostat and this verified the liquid helium data. This method now allows detection of ultra small leaks with liquid helium.

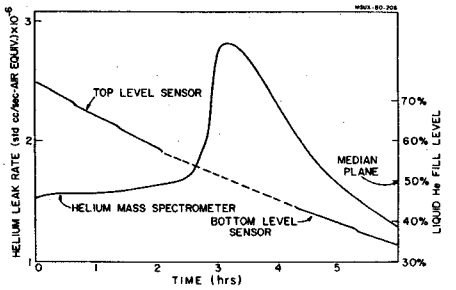

FIG. 3. The helium concentration in the vacuum jacket and the decreasing liquid level as a function of time are given. Above the median plane, the helium concentration is constant. At the median plane the helium concentration increases by 2 and then decreases. This change in helium concentration is attributed to uncovering a leak channel in the cryostat by the liquid helium.

Phase II Liquid Helium Refrigerator-Liquifier

M. Mallory, H. Blosser, P. Brindza and H. Laumer

The liquid helium refrigerator-liquifier for Phase II was specified and procured during the last year. The major refrigerator performance specification is listed in Table I. Cryogenic Consultants Inc., was the successful bidder and are now completing the design. Figure 1, is the mass flow diagram of the helium system and Fig. 2 is the corresponding temperature entropy diagram. Figure 3 is the general layout and final assembly of the cold box. The helium screw compressor (from Sullair Refrigeration Inc.) provides 62 g/sec at 250 psi. The 2500 ℓ dewar will be from Gardner Cryogenics Inc., a division of Air Products Inc. The cold box, consisting of heat exchangers and all associated valving and piping will be constructed by Meyer Tool and Manufacturing Inc.

Table I. Refrigerator performance specifications.

Watts	l/Hr	LN_2 Consumption	Cooldown Mass Flow
200 W	50 l/hr	--	--
400 W	100 l/hr	47 l/hr	--
200 W	50 l/hr	228 l/hr	15 gm/sec

MSUX-80-544

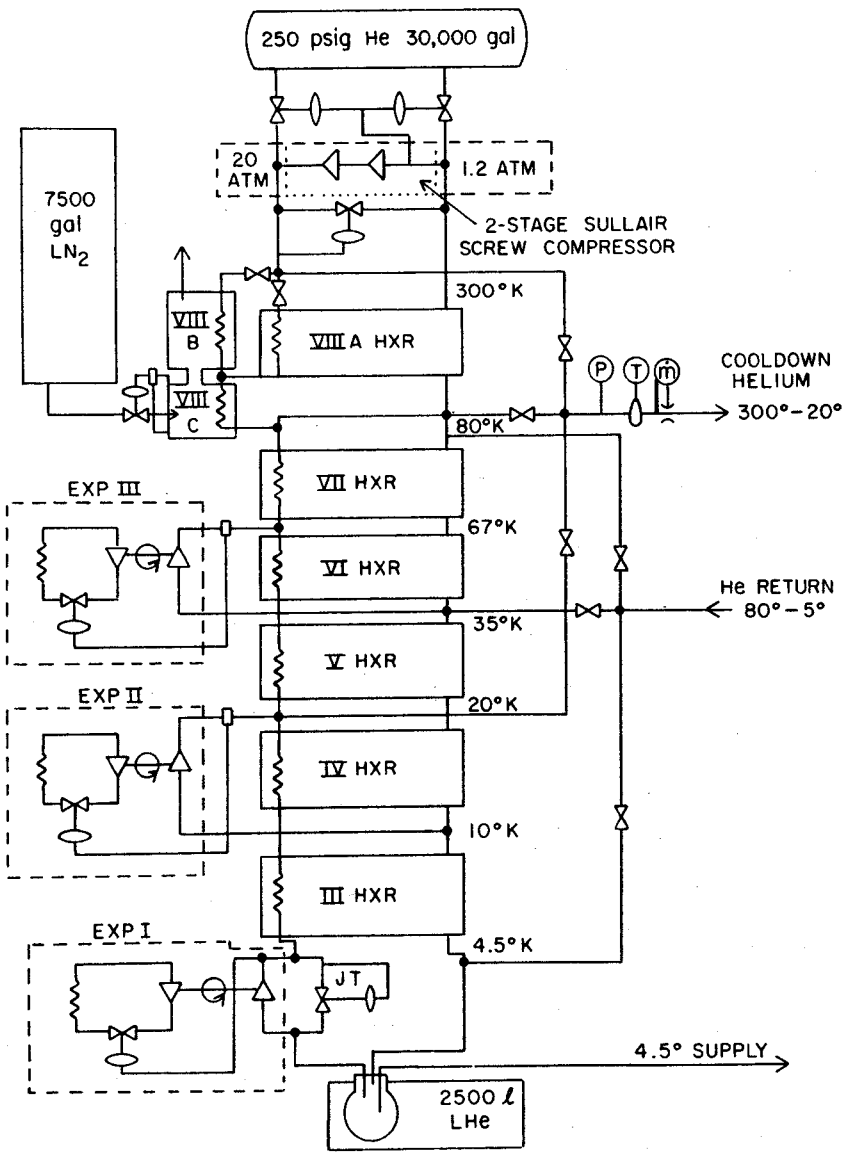

FIG. 1

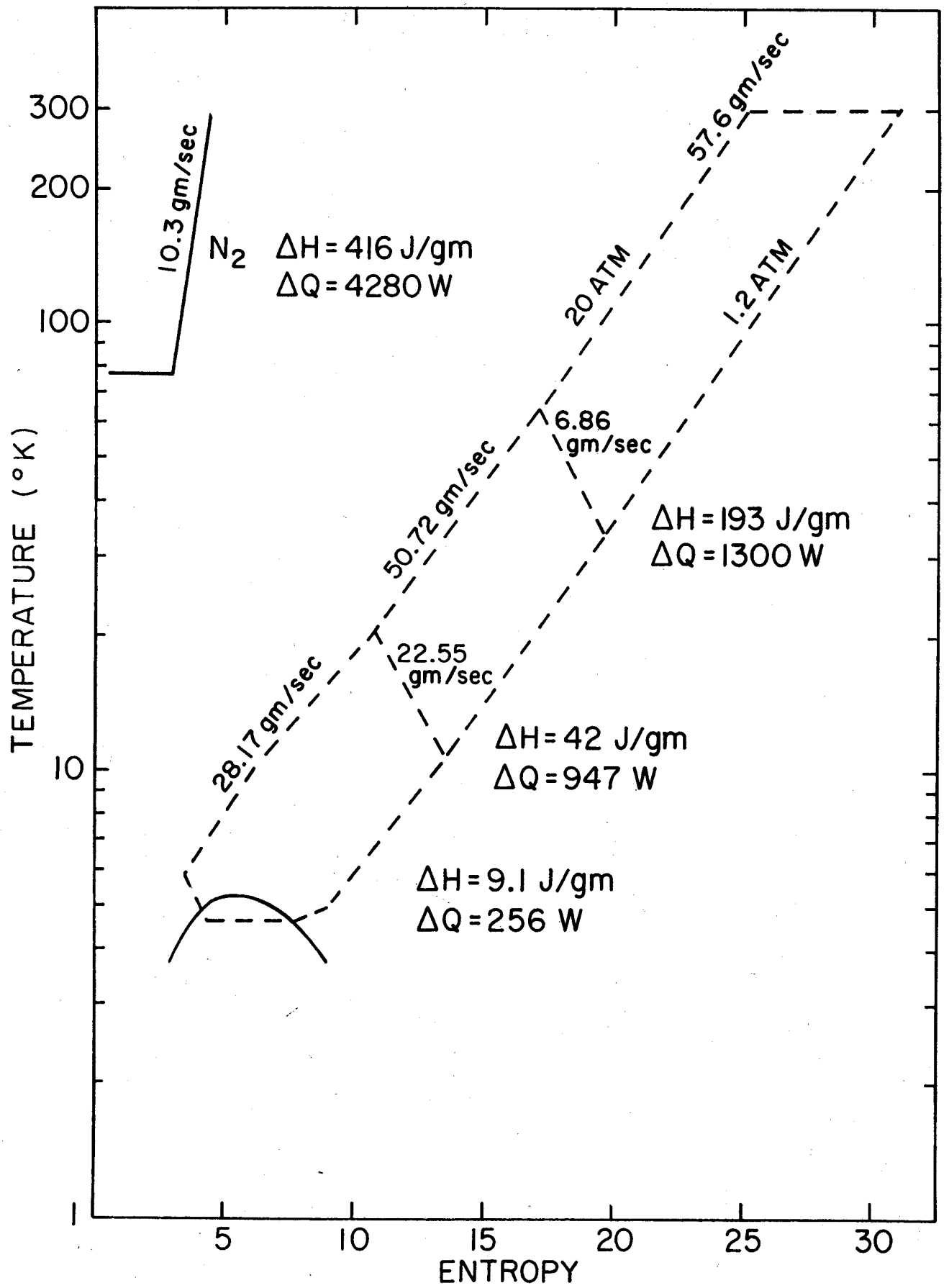
300
200
100
10
1
TEMPERATURE (°K)
5
10
15
20
25
30
ENTROPY
10.3 gm/sec
N2 ΔH = 416 J/gm
ΔQ = 4280 W
57.6 gm/sec
20 ATM
1.2 ATM
6.86 gm/sec
50.72 gm/sec
ΔH = 193 J/gm
ΔQ = 1300 W
22.55 gm/sec
28.17 gm/sec
ΔH = 42 J/gm
ΔQ = 947 W
ΔH = 9.1 J/gm
ΔQ = 256 W

Figure 2

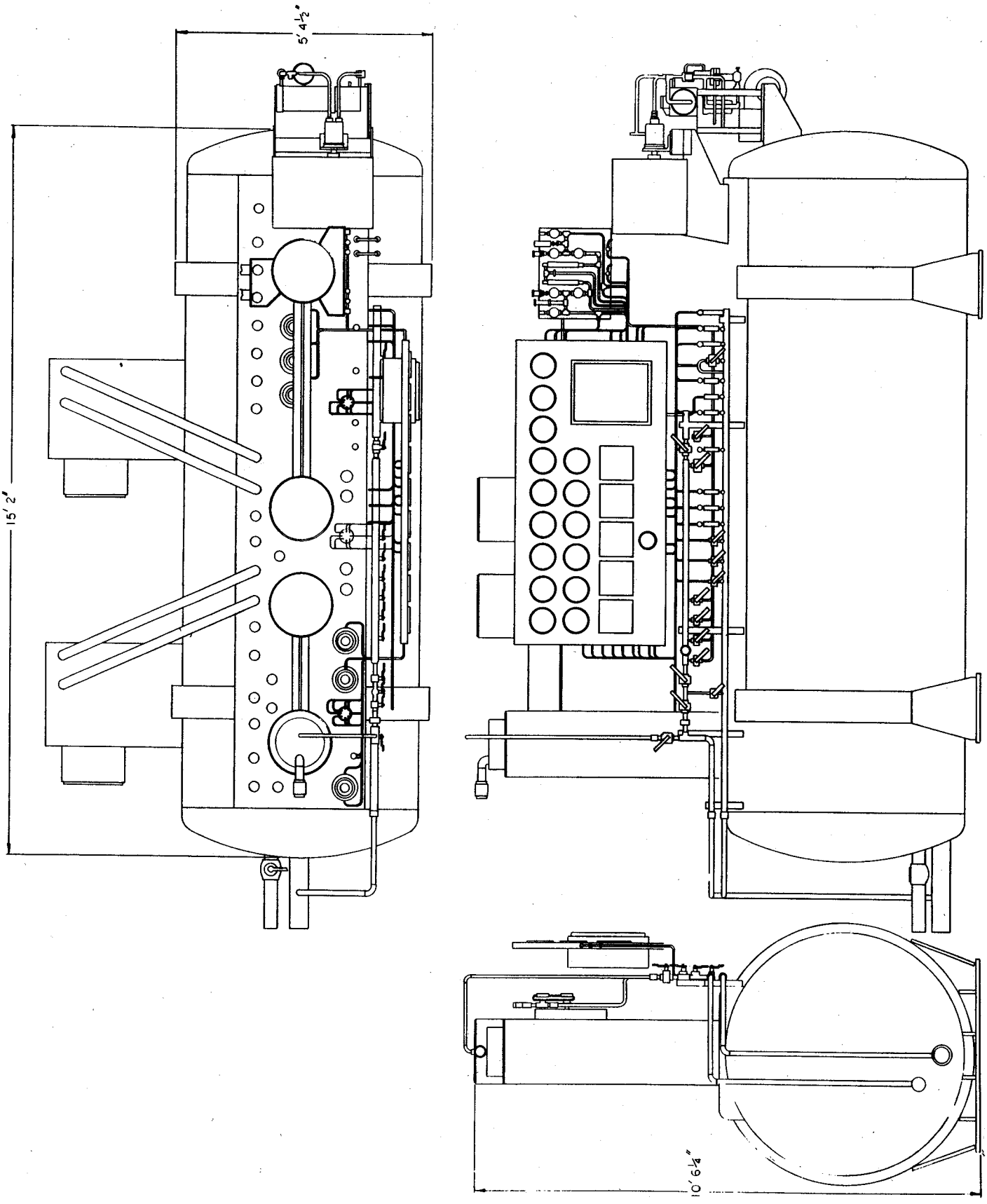

Figure 3

The compressors will arrive Nov. 1, 1980, the dewar Dec. 1, 1980 and the cold box April 1, 1981. A 30,000 gallon ambient temperature helium gas reservoir has been procured and will be delivered in late 1980.

In addition to the helium system, the LN_2 system is also being enlarged. Two surplus LN_2 tanks of 3600 gallons each have been purchased and are being rennovated. This system will provide 100 gm/sec of LN_2 and 7200 SCFH of dry N_2 gas. Figure 4 is a site layout for the cryogenic components.

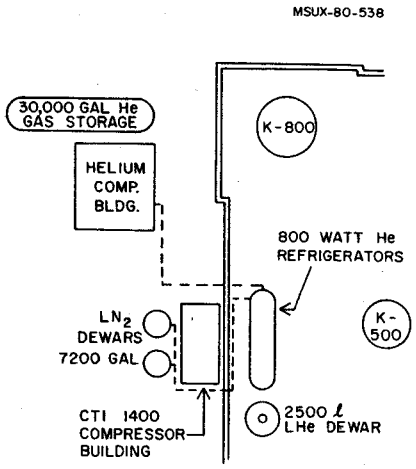

FIG. 4